Noradrenaline release from the locus coeruleus shapes stress-induced hippocampal gene expression

Mattia Privitera[1,2], Lukas M. von Ziegler[1,2], Amalia Floriou-Servou[1,2], Sian N. Duss[1,2], Runzhong Zhang[1], Rebecca Waag[1,2], Sebastian Leimbacher[1], Oliver Sturman[1,2], Fabienne K. Roessler[1], Annelies Heylen[3], Yannick Vermeiren[3,4], Debby Van Dam[3,5], Peter P. De Deyn[3,5,6], Pierre-Luc Germain[1,2,7,8] & Johannes Bohacek[1,2#]

[1] Laboratory of Molecular and Behavioral Neuroscience, Institute for Neuroscience, Department of Health Sciences and Technology, ETH Zurich, Switzerland
[2] Neuroscience Center Zurich, ETH Zurich and University of Zurich, Switzerland
[3] Laboratory of Neurochemistry and Behavior, Experimental Neurobiology Unit, Department of Biomedical Sciences, University of Antwerp, Wilrijk (Antwerp), Belgium
[4] Division of Human Nutrition and Health, Chair Group of Nutritional Biology, Wageningen University & Research (WUR), Wageningen, Netherlands.
[5] Department of Neurology and Alzheimer Center, University of Groningen and University Medical Center Groningen (UMCG), Groningen, Netherlands
[6] Department of Neurology, Memory Clinic of Hospital Network Antwerp (ZNA) Middelheim and Hoge Beuken, Antwerp, Belgium
[7] Computational Neurogenomics, Institute for Neuroscience, Department of Health Sciences and Technology, ETH Zürich, Zurich, Switzerland.
[8] Laboratory of Statistical Bioinformatics, University of Zürich, Switzerland

 # Corresponding Author: Johannes Bohacek, johannes.bohacek@hest.ethz.ch

Keywords
transcriptome, hippocampus, locus coeruleus, noradrenaline, norepinephrine, stress response, optogenetics, anxiety, thyroid hormone, Dio2

Author contributions:
Mattia Privitera: conceived experiments, conducted experiments, sample processing, data analysis, graphs & figures, interpreted results, wrote manuscript
Lukas von Ziegler: conducted experiments, data analysis, graphs & figures, interpreted results, wrote manuscript
Amalia Floriou-Servou: conceived experiments, conducted experiments
Sian Duss: conceived experiments, conducted experiments
Runzhong Zhang: conducted experiments, sample processing
Rebecca Waag: conducted experiments, sample processing
Sebastian Leimbacher: conducted experiments, data analysis
Oliver Sturman: conducted experiments
Fabienne Rössler: data analysis
Yannick Vermeiren: sample processing, data analysis (uHPLC)
Annelies Heylen: sample processing, data analysis (uHPLC)
Debby Van Dam: sample processing, data analysis (uHPLC), provided resources and funding (uHPLC)
Peter P. De Deyn: provided resources and funding (uHPLC)
Pierre-Luc Germain: conducted data analysis, created graphs & figures, wrote manuscript
Johannes Bohacek: conceived experiments, interpreted results, provided resources and funding, wrote manuscript

Abstract
Exposure to an acute stressor triggers a complex cascade of neurochemical events in the brain. However, deciphering their individual impact on stress-induced molecular changes remains a major challenge. Here we combine RNA-sequencing with selective pharmacological, chemogenetic and optogenetic manipulations to isolate the contribution of the locus coeruleus - noradrenaline (LC-NA) system to the acute stress response. We reveal that NA-release during stress exposure regulates a large and reproducible set of genes in the dorsal and ventral hippocampus via β-adrenergic receptors. For a smaller subset of these genes, we show that NA release triggered by LC stimulation is sufficient to mimic the stress-induced transcriptional response. We observe these effects in both sexes, and independent of the pattern and frequency of LC activation. Using a retrograde optogenetic approach, we demonstrate that hippocampus-projecting LC neurons directly regulate hippocampal gene expression. Overall, a highly selective set of astrocyte-enriched genes emerges as key targets of LC-NA activation, most prominently several subunits of protein phosphatase 1 (*Ppp1r3c*, *Ppp1r3d*, *Ppp1r3g*) and type II iodothyronine deiodinase (*Dio2*). These results highlight the importance of astrocytic energy metabolism and thyroid hormone signaling in LC-mediated hippocampal function and offer new molecular targets for understanding how NA impacts brain function in health and disease.

Introduction
When an organism faces an acutely stressful situation, a set of evolutionarily conserved mechanisms are triggered to re-route all available resources to body functions that enhance performance and increase the chance of survival (Floriou-Servou et al. 2021; Joëls and Baram 2009). In the brain, stress exposure immediately activates the locus coeruleus-noradrenaline (LC-NA) system. Although the LC is a heterogeneous structure with modular organization, it appears that in stressful situations, broad activation of the LC - and subsequent widespread NA release throughout the brain - serves as a broadcast signal to orchestrate re-routing of computational resources to meet situational demands (Likhtik and Johansen 2019; Poe et al. 2020). On the network level, for example, NA release from the LC is sufficient to trigger a rapid reconfiguration of large-scale networks that shift processing capacity towards salience processing (Zerbi et al. 2019; Oyarzabal et al. 2022). On a circuit level, forebrain regions seem to be particularly important targets of the LC-NA system to influence cognitive processes and ultimately behavior. This involves the engagement of anxiety and memory circuits including the amygdala, hippocampus and prefrontal cortex, which leads to an increase in avoidance behavior (McCall et al. 2015, 2017; Hirschberg et al. 2017; Zerbi et al. 2019) and supports memory formation of salient events (Uematsu, Tan, and Johansen 2015; Hansen 2017; Sara 2015; Schwabe et al. 2022).
While the insights into network and circuit dynamics of the LC have been galvanized by recent advances in circuit neuroscience tools, our understanding of the molecular impact of NA release has remained largely unexplored. However, we know that the stress response triggers multifaceted molecular cascades that profoundly change brain function and behavior in response to stressful events (Floriou-Servou et al. 2021; Joëls and Baram 2009). These molecular changes are mediated by a large number of neurotransmitters, neuropeptides and hormones, which operate on different time scales, to allow rapid activation, sustained activity and successful termination of the stress response. Many of the rapid molecular changes induced by stress exposure seem to be driven by NA. For example, several of the genes that are induced by an acute stress challenge can be blocked by β-adrenergic receptor antagonists (Roszkowski et al. 2016). However, a similar analysis on the genome-wide level has not been conducted. Further, it remains unknown whether NA release alone is sufficient to trigger transcriptomic changes in the first place. Here, we profile the molecular fingerprint of stress-induced NA release by combining pharmacologic, chemogenetic and optogenetic manipulation of the LC-NA system with genome-wide transcriptomic analyses. We focus on the hippocampus, as it receives its sole NA supply from the LC (Loy et al. 1980; Robertson et al. 2013; Oleskevich, Descarries, and Lacaille 1989), and because the molecular response to acute stress has been

characterized in great detail in this region (von Ziegler et al. 2022; Mifsud et al. 2021; Floriou-Servou et al. 2018). As the dorsal hippocampus (dHC) and ventral hippocampus (vHC) are involved in different circuits (Strange et al. 2014) and are transcriptionally very distinct (Cembrowski et al. 2016; Floriou-Servou et al. 2018), we analyze these regions separately.

Results

A recent multi-omic characterization of the acute stress response in the mouse hippocampus revealed that stress-induced transcriptional changes peak between 45-90 min after stress exposure, before gradually returning to baseline (von Ziegler et al. 2022). To determine how NA might contribute to these effects, we first measured the dynamics of NA turnover in response to a cold swim stress exposure in the brain. Using ultra-high performance liquid chromatography (uHPLC), we determined concentrations of NA and its main metabolite 3-Methoxy-4-hydroxyphenylglycol (MHPG) at various time points over 3 hours after swim stress exposure in the cortex (Fig. 1a). NA turnover (as measured by the MHPG/NA ratio) peaked at 45 min and returned to baseline within 90 min after stress onset (Fig. 1b). Therefore, we chose the 45 min time point to assess the contribution of NA signaling to stress-induced transcriptomic changes. To this end, we blocked adrenergic receptors using either the α1-adrenergic receptor antagonist prazosin, or the β-adrenergic receptor antagonist propranolol prior to stress exposure (Fig. 1c). In line with our previous work (von Ziegler et al. 2022; Floriou-Servou et al. 2018; Roszkowski et al. 2016), acute swim stress induced a robust transcriptional response 45 min after stress exposure in both dorsal hippocampus (dHC) and ventral hippocampus (vHC) (see Veh-C vs Veh-S in Fig. 1d, Supplementary Fig. 1a). Prazosin only mildly impacted stress-dependent transcriptional changes in the dHC and vHC (see Veh-S vs Pra-S in Fig. 1d, Supplementary Fig. 1a). Surprisingly, in stress-exposed animals prazosin seemed to slightly amplify - rather than prevent - some stress effects (Supplementary Fig. 1b). In contrast, propranolol had a profound impact, preventing many of the stress-induced changes in the dHC and vHC (see Veh-S vs Pro-S in Fig. 1d, Supplementary Fig. 1a). Indeed, a direct comparison between the stress group and the stress + propranolol group found many genes that were significantly altered by propranolol administration (Fig. 1e, Supplementary Fig. 1c). This response to propranolol was very similar in the dHC and vHC (Fig. 1e).

While blocking β-adrenergic receptors was able to block stress-induced gene expression, we did not test whether propranolol might decrease gene expression already at baseline, independent of stress. Additionally, all tests had thus far been conducted in male mice, raising the question about potential sex differences in NA-mediated transcriptomic responses. To address these two issues, we repeated the experiment in both sexes and included a group that received a propranolol injection but was not exposed to stress (Fig. 1f). Combining the data from both experiments, we repeated the analysis for each region, to identify genes whose response to stress was inhibited by propranolol (Figure 1g). As in the previous experiment, we found that many of the stress-induced gene expression changes were blocked by propranolol injection in both dHC (Figure 1g, left panel) and vHC (Figure 1g, right panel). Importantly, propranolol did not change the expression level of these genes in the absence of stress. We then directly compared the genes sensitive to stress and propranolol treatment in both dHC and vHC. To this end, we plotted the union of genes showing a significant stress:propranolol interaction in either region in one heatmap across both dHC and vHC (Supplementary Figure 1d). This showed again that the stress-induced changes were very similar in dHC and vHC, and that propranolol similarly blocked many of them. Finally, we asked whether the response differs between males and females. Despite clear sex differences in gene expression at baseline (data not shown), we found no significant sex differences in response to stress or propranolol between male and female mice (FDR<0.05; Fig. 1g). To more directly visualize this, we compared females and males by plotting the log2-fold changes of the stress:propranolol interaction across all stress-induced genes that were blocked by propranolol. We find very similar regulation patterns in both sexes (Figure 1h). Although none of these sex differences are significant, some genes seem to show quantitative differences, so we plotted the expression patterns of the 5 genes showing the largest difference

in interaction term as box-plots, which suggest that these spurious differences are likely due to noisy coefficient estimates (Supplementary Fig. 1e). To address concerns that our analysis of sex differences might not have been sufficiently powered, we performed a meta-analysis of the experiments shown here along with previously published datasets from our lab (Floriou-Servou et al. 2018; von Ziegler et al. 2022). In all these experiments, the vHC of male and female mice was profiled 45 min after exposure to an acute swim stress challenge. This resulted in a sample size of 51 males and 20 females. Despite this high number of independent samples, we could not identify any statistically significant interaction between sex and the stress response. To identify candidates that might not reach significance while discounting differences due to noise in fold-change estimates, we reproduced the same analysis using DESeq2 with Approximate Posterior Estimation for generalized linear model (apeglm) logFC shrinkage (A. Zhu, Ibrahim, and Love 2018). This analysis also did not reveal any sex differences in the stress response (Supplementary Fig. 1f). We then tailored the meta-analysis specifically to the set of stress-responsive genes that were blocked by propranolol, and also for these genes the response to stress was strikingly similar in both sexes (Supplementary Fig. 1g). Altogether, we conclude that there are no major sex differences in the rapid transcriptomic stress response in the hippocampus, and that blocking beta-receptors prevents a large set of stress-induced genes in both females and males.

We then tested whether direct activation of hippocampal β-adrenergic receptors is sufficient to induce gene expression changes. To this end, we infused animals with the β-adrenergic receptor agonist isoproterenol into the dHC (because it is easier to target than the vHC). We then manually selected a few genes whose stress-induced induction was blocked by propranolol pre-treatment either partially (*Apold1*), or completely (*Dio2*, *Sik1* and *Ppp1r3c*; see Figure 1g), and assessed the expression of these genes by targeted qRT-PCR assays (Supplementary Fig. 1h). Isoproterenol directly increased hippocampal expression of *Apold1*, *Dio2* and *Sik1, but not Ppp1r3c* (Supplementary Fig. 1i). In summary, the results presented here show that for a large number of genes, NA signaling via β-adrenergic receptors is required to regulate the stress-induced transcriptional response.

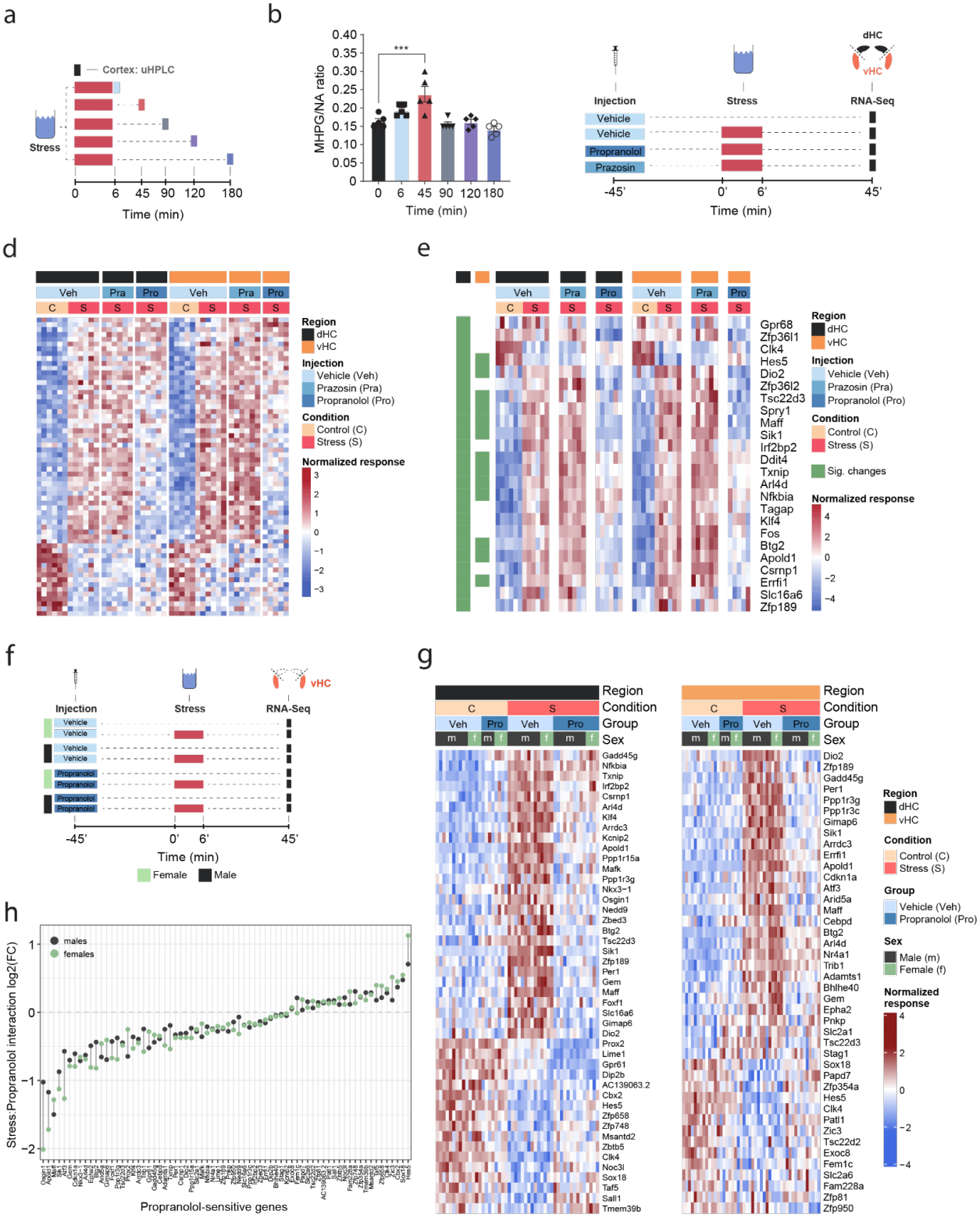

Fig. 1: β-adrenergic receptors mediate stress-induced transcriptomic changes in the hippocampus and are independent of subregion and sex. a, Experimental design for assessing stress-induced cortical noradrenaline (NA) turnover at various time points following stress exposure. **b**, Stress-dependent changes in cortical NA turnover, as measured by the ratio of 3-Methoxy-4-hydroxyphenylglycol (MHPG) and NA levels. NA turnover significantly increased

within 45 min and returned to baseline within 90 min of stress onset (one-way ANOVA with Tukey's post hoc tests; $F(5, 24) = 10.55$, $p < 0.0001$). $n = 5$ per group and individual data points are shown with bars representing mean ± s.e.m. **c**, Experimental design for assessing the effect of prazosin (Pra, 1 mg/kg, i.p.) and propranolol (Pro, 10 mg/kg, i.p.) on stress-dependent transcriptomic changes in the dorsal (dHC) and ventral (vHC) hippocampus 45 min after stress exposure. **d**, Heatmap showing all differentially expressed genes across dHC and vHC and pharmacological treatments 45 min after acute swim stress exposure. $n = 6$ per group. **e**, Heatmap selectively showing those stress-responsive genes that are affected by the β-adrenergic receptor antagonist propranolol 45 min after acute swim stress exposure in the dHC and vHC (FDR-adjusted $p < 0.05$). **f**, Experimental design for assessing propranolol-dependent changes in the vHC of female and male mice. $n = 5$ per group. **g**, Heatmap showing - across the two experiments - the expression of all stress-dependent genes that are affected by propranolol treatment in either region (dHC and vHC; FDR-adjusted $p < 0.05$). **h**, Comparison of the modulating effect of propranolol on the stress response (log2-fold-changes of the stress:propranolol interaction term) in males and females, across both experiments and regions.

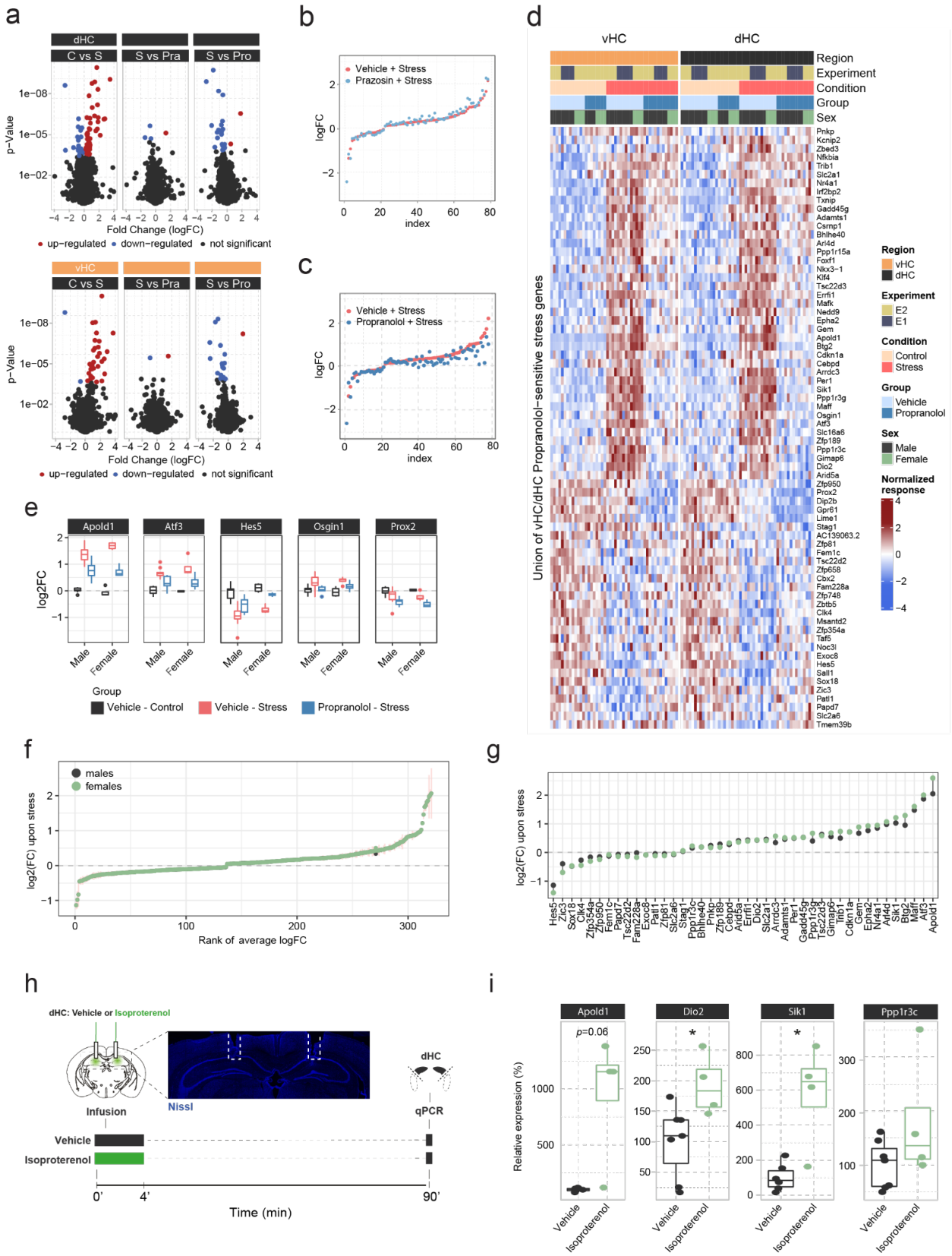

Supplementary Figure 1. In-depth analysis of noradrenergic contribution to stress-induced transcriptomic changes in the hippocampus. a, Volcano plots showing differentially expressed RNA transcripts between vehicle

(Veh, i.p.), prazosin (Pra, 1 mg/kg, i.p.) and propranolol (Pro, 10 mg/kg, i.p.) injected animals 45 min after onset of acute swim stress exposure. Red and blue values represent changes with FDR-adjusted $p<0.05$ ($n = 6$ per group). **b**, Strength of the prazosin effect on the transcriptomic stress response. Data are sorted by interaction strength in the stress group (orange) and the corresponding interaction strength of the stress+prazosin group are shown in lightblue for the same gene. **c**, Strength of the propranolol effect on the transcriptomic stress response. Data are sorted by interaction strength in the stress group (orange) and the corresponding interaction strength of the stress+prazosin group are shown in dark blue for the same gene. **d**, Heatmap showing expression, across both experiments and regions, of all stress genes with a significant stress:propranolol interaction. **e**, Expression (in the vHC) of the genes from Figure 1h showing the largest differences (none statistically significant) in the stress:propranolol interaction term between males and females. **f**, Comparison of the transcriptomic changes 45min after stress between males and females, in a meta-analysis of 71 vHC samples. The fold-change estimates were obtained using DESeq2 with apeglm-shrinkage (A. Zhu, Ibrahim, and Love 2018). Vertical bars show the standard error of the fold-change estimates. **g**, (Unshrunk) fold-change estimates of propranolol-sensitive genes upon stress in males and females, based on the meta-analysis. **h**, Experimental design for assessing the effect of intrahippocampal infusion of isoproterenol (3 µg/hemisphere) on expression of selected genes in the dorsal hippocampus (dHC) 90 min after infusion in the absence of stress. Representative image shows the cannula placement (dashed line) in the dHC stained by Nissl (blue) **i**, Boxplots showing the expression of selected stress- and propranolol-responsive genes (*Apold1, Dio2 and Sik1*) 90 min after infusion of isoproterenol (3 µg/hemisphere) into the dHC, as measured by quantitative real-time PCR. Isoproterenol increased the expression of *Dio2* (unpaired t test; $t(9) = 2.637$, $p = 0.02706$) and *Sik1* (welch unpaired t test; $t(3.3) = 3.176$, $p = 0.04428$). Vehicle, $n = 7$; Isoproterenol, $n = 4$. $^*p < 0.05$.

An acute stress exposure triggers the release of a plentitude of stress mediators - neurotransmitters, peptides and hormones - that interact to regulate molecular changes (Joëls and Baram 2009). As it is unclear how NA interacts with other stress mediators, we asked whether we could isolate the molecular changes for which NA release is not only required, but sufficient, by triggering NA release in the hippocampus. Because hippocampal NA supply is provided exclusively by long-range projections from the LC (Loy et al. 1980; Robertson et al. 2013; Oleskevich, Descarries, and Lacaille 1989), we first pharmacologically activated NA release using the α2-adrenergic receptor antagonist yohimbine, which strongly disinhibits noradrenergic neurons (Fig. 2a). As expected, systemic administration of yohimbine (3 mg/kg, i.p.) led to a strong increase in cFos expression within the LC (Fig. 2b) and increased NA turnover in the cortex (Supplementary Fig. 2a). Because NA mediates the stress-induced increase in anxiety (McCall et al. 2015; Zerbi et al. 2019), we also evaluated behavioral changes in the open field test. We had shown previously that acute stress increases anxiety in the open field test (Sturman, Germain, and Bohacek 2018; von Ziegler et al. 2022) (Supplementary Fig. 3a), and very similarly yohimbine also suppressed locomotion and exploratory behaviors (Supplementary Fig. 3b). To directly compare the impact of stress and yohimbine injection on the transcriptomic response in the hippocampus, we then exposed mice to acute swim stress, or to yohimbine injection without stress exposure (Fig. 2c). Yohimbine induced a clear and consistent transcriptional response in the dHC and vHC. Direct comparison between stress and yohimbine revealed no significant differences (Fig. 2d-e, Supplementary Fig. 2b), suggesting that yohimbine administration alone can mimic a large fraction of the stress-induced transcriptional response. To more specifically probe whether selective activation of the LC-NA system alone is sufficient to trigger the observed changes in gene expression, we turned to direct activation of the LC. First, we used the chemogenetic actuator hM3Dq (H. Zhu et al. 2016) to trigger a strong and prolonged activation of the LC (Fig. 2f). In support of previous work (Zerbi et al. 2019; Privitera et al. 2020), injection of an ultra-low dose of the potent hM3Dq-actuator clozapine (0.03 mg/kg) led to a strong cFos increase in tyrosine hydroxylase (TH) positive LC neurons in hM3Dq+, but not in hM3Dq- animals (Fig. 2g). Further, we used fiber photometry combined with genetically encoded NA sensors to measure NA release in real time directly in the hippocampus (Kagiampaki et al. 2023; Grimm et al. 2022; Feng et al. 2019). We found that chemogenetic LC activation leads to a rapid and sustained increase in hippocampal NA in both females and males (Supplementary Figure 2c-e).

Behaviorally, chemogenetic LC activation induced an anxiety-like phenotype in the open field test, similar to the response to yohimbine (Supplementary Fig. 3c). Transcriptomic analysis revealed that chemogenetic LC activation induced significant transcriptomic changes that were similar in the dHC and vHC (Fig. 2h). Overall, these transcriptional changes affected fewer genes than those observed after systemic noradrenergic activation by yohimbine administration.

Despite its specificity, chemogenetic LC activation does not provide the temporal control to restrict LC activation to shorter periods of time. Thus, we repeated the experiment using optogenetic LC activation (Fig. 2i). To demonstrate that optogenetic LC activation directly triggers NA release in the hippocampus, we combined it with fiber photometry recordings using NA sensors (Supplementary Figure 2f). We found that short (10 sec) activation with 5 Hz triggered an almost instantaneous, sharp increase in hippocampal NA release in both females and males (Supplementary Figure 2g-h). To mimic stress-induced LC activity, LC neurons were unilaterally stimulated with 5 Hz in a 3 min off/on paradigm for 21 min, which has previously been shown to phenocopy stress-induced effects on behavior in mice (McCall et al. 2015, 2017). Again, tissue was collected 45 min after the start of stimulation, and in a separate cohort also 90 min afterwards, to study how LC-mediated transcriptomic responses evolve over time. Optogenetic LC activation led to a significant cFos increase only in the stimulated LC hemisphere of ChR2+ animals, and these changes were significant at both time points (Fig. 2j). Stimulated ChR2+ animals also showed a significant increase in the MHPG/NA ratio 45 and 90 min after stimulation onset compared to controls (Fig. 2k). Additionally, we found that tonic 5 Hz activation of the LC led to immediate pupil dilation in ChR2+, but not in ChR2- animals (Fig. 2l), as previously described (Privitera et al. 2020). Unilateral 5 Hz stimulation also reduced exploratory rearing behaviors in ChR2+ animals in the open field test (Supplementary Fig. 3d). Similar to the effects of acute stress and chemogenetic LC activation, unilateral 5 Hz stimulation of the LC induced significant transcriptomic changes at the 45 min time point in the ipsilateral vHC of ChR2+ mice compared to controls (Fig. 2m). Notably, most of these changes disappeared again 90 min after stimulation onset, indicating that the LC-NA system mainly induces an early wave of transcriptomic changes in the hippocampus, which are not maintained over longer periods of time.

Next, we leveraged the extensive transcriptional data presented thus far to test which genes were consistently responsive to the various manipulations of the LC-NA system across experiments. First, we compared gene expression changes induced by yohimbine, chemogenetic and optogenetic LC activation in the vHC. This allowed us to identify a small set of genes that are very consistently regulated across all modes of LC activation (Fig. 2n). Second, we ranked genes across all the transcriptomic experiments according to their responsiveness to NA manipulations (based on p-value). This analysis includes acute stress exposure with pharmacological inhibition of NA receptors, as well as yohimbine treatment, chemogenetic and optogenetic LC activation. We then calculated the cumulative rank for each gene across all experiments to find genes with the most consistent response to NA manipulations (Supplementary Table 1). This analysis reproduced most of the genes identified in Figure 2n, and additionally revealed more genes with particularly robust changes in response to LC-NA manipulations across experiments (Fig. 2o, Supplementary Fig. 4). The top 10 genes were *Dio2*, *Ppp1r3c*, *Ppp1r3g*, *Sik1*, *Tsc22d3*, *Ppp1r3d*, *F3*, *Sertad1*, *Nr4a1* and *Timp3*. For visualization, the top 4 of these genes are shown across all LC-NA manipulations in Supplementary Fig. 4. Going forward, we use these 10 transcripts as a *bona fide* list of LC-NA-responsive genes.

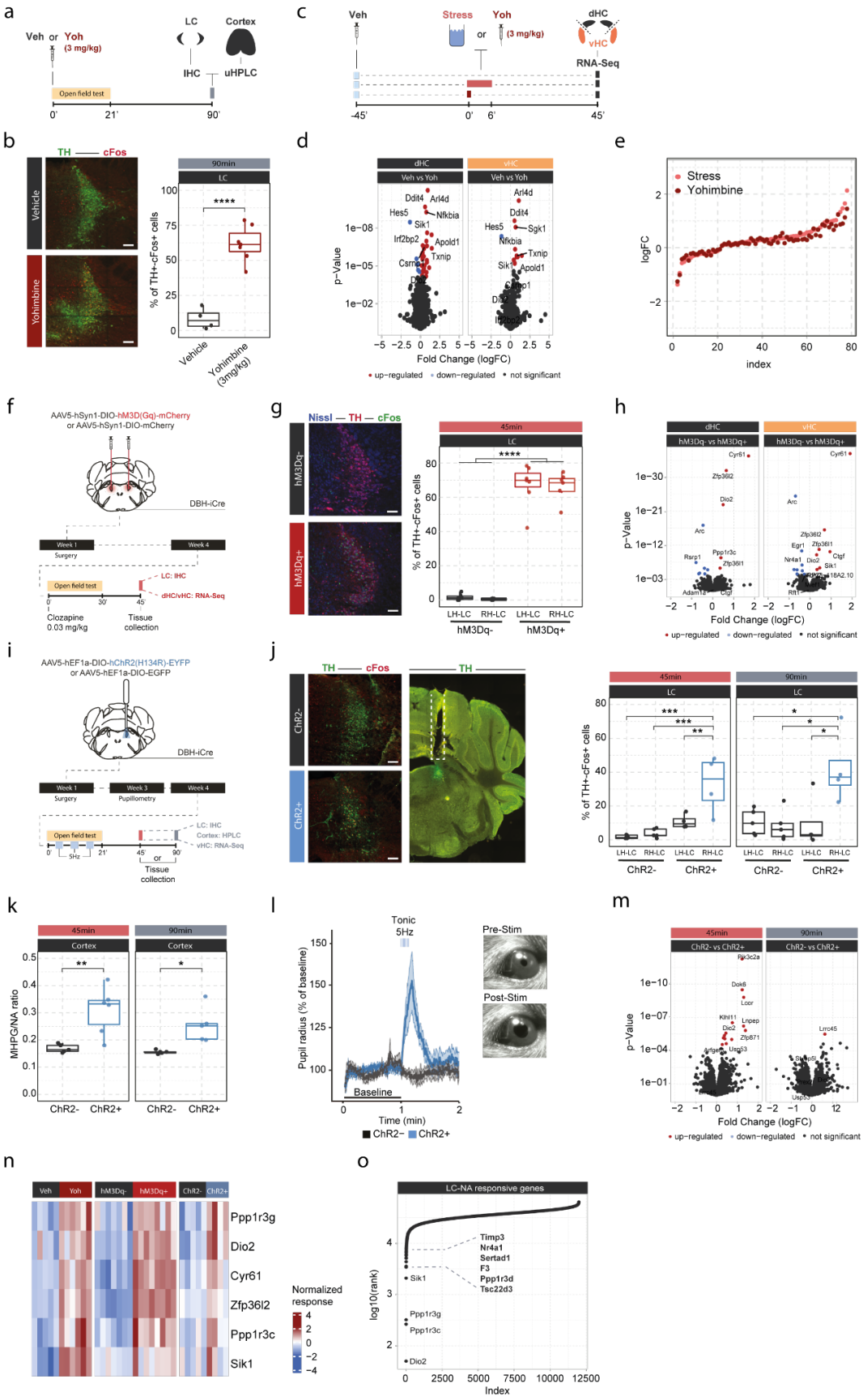
a
Veh or Yoh (3 mg/kg)
LC
Cortex
IHC
uHPLC
Open field test
0'
21'
90'
b
TH — cFos
Vehicle
Yohimbine
90min
LC
% of TH+-cFos+ cells
Vehicle
Yohimbine (3mg/kg)
c
Veh
Stress
Yoh
or
(3 mg/kg)
dHC
vHC
RNA-Seq
-45'
0'
6'
45'
d
dHC
vHC
Veh vs Yoh
p-Value
Fold Change (logFC)
up-regulated
down-regulated
not significant
e
Stress
Yohimbine
logFC
index
f
AAV5-hSyn1-DIO-hM3D(Gq)-mCherry
or AAV5-hSyn1-DIO-mCherry
DBH-iCre
Week 1
Week 4
Surgery
Open field test
LC: IHC
dHC/vHC: RNA-Seq
Clozapine 0.03 mg/kg
Tissue collection
g
Nissl — TH — cFos
hM3Dq-
hM3Dq+
45min
LC
% of TH+-cFos+ cells
LH-LC
RH-LC
h
dHC
vHC
hM3Dq- vs hM3Dq+
p-Value
Fold Change (logFC)
up-regulated
down-regulated
not significant
i
AAV5-hEF1a-DIO-hChR2(H134R)-EYFP
or AAV5-hEF1a-DIO-EGFP
DBH-iCre
Week 1
Week 3
Week 4
Surgery
Pupillometry
Open field test
LC: IHC
Cortex: HPLC
vHC: RNA-Seq
Tissue collection
j
TH — cFos
TH
ChR2-
ChR2+
45min
90min
LC
% of TH+-cFos+ cells
LH-LC
RH-LC
ChR2-
ChR2+
k
45min
90min
Cortex
MHPG/NA ratio
ChR2-
ChR2+
l
Tonic 5Hz
Pre-Stim
Post-Stim
Pupil radius (% of baseline)
Baseline
Time (min)
ChR2−
ChR2+
m
45min
90min
ChR2- vs ChR2+
p-Value
Fold Change (logFC)
up-regulated
down-regulated
not significant
n
Veh
Yoh
hM3Dq-
hM3Dq+
ChR2-
ChR2+
Ppp1r3g
Dio2
Cyr61
Zfp36l2
Ppp1r3c
Sik1
Normalized response
o
LC-NA responsive genes
log10(rank)
Timp3
Nr4a1
Sertad1
F3
Ppp1r3d
Tsc22d3
Sik1
Ppp1r3g
Ppp1r3c
Dio2
Index

Fig. 2: Locus Coeruleus-mediated transcriptomic changes in the hippocampus. a, Experimental design for assessing LC activation and cortical NA release induced by injection of yohimbine (3 mg/kg, i.p.). **b**, Representative images and quantification of LC activation in mice 90 min after injection of vehicle or yohimbine as measured by cFos (red) and tyrosine hydroxylase (TH, green) coexpression within LC neurons. Yohimbine injection increased cFos expression within LC neurons compared to vehicle-injected animals (unpaired t test; t(8.9) = -8.814, p = 1.083e-05). Vehicle, n = 4; Yohimbine n = 7. Scale bar: 100µm. **c**, Experimental design for comparing molecular changes in the hippocampus after acute swim stress exposure or yohimbine administration. **d**, Volcano plots showing differentially expressed RNA transcripts in the dorsal (dHC) and ventral (vHC) hippocampus between control (Veh) and yohimbine (Yoh) injected animals 45 min after injection. Red and blue values represent changes with FDR-adjusted p<0.05 (Veh n = 6, Yoh n = 6). **e**, Strength of the yohimbine effect in comparison to the transcriptomic stress response. Data are sorted by interaction strength in the stress group (orange) and the corresponding interaction strength of the yohimbine group are shown in dark red for the same gene. **f**, Experimental design for assessing LC activation and hippocampal transcriptomic changes induced by chemogenetic LC activation. **g**, Representative images and quantification of LC activation in mice 45 min after injection of clozapine (0.03 mg/kg) in hM3Dq- and hM3Dq+ animals as measured by cFos (green) and tyrosine hydroxylase (TH, red) coexpression within LC neurons. Neurons are stained with Nissl (blue). Clozapine injection increased cFos expression within LC neurons in hM3Dq+ animals compared to hM3Dq- animals (one way ANOVA; F(3, 23) = 135.4, p = 9.34e-15). hM3Dq- n = 6, hM3Dq+ n = 7. Scale bar: 100µm. **h**, Volcano plots showing differentially expressed RNA transcripts between hM3Dq- and hM3Dq+ animals 45 min after injection of clozapine (0.03 mg/kg) in the dHC and vHC. Red and blue values represent changes with FDR-adjusted p<0.05 (hM3Dq- n = 6, hM3Dq+ n = 7). **i**, Experimental design for assessing LC activation, cortical NA release, pupillometry and hippocampal transcriptomic changes induced by optogenetic 5 Hz LC activation. **j**, Representative images and quantification of LC activation in mice after 5 Hz optogenetic LC activation as measured by cFos (red) and tyrosine hydroxylase (TH, green) coexpression within LC neurons in stimulated and non-stimulated LC hemispheres of ChR2- and ChR2+ animals. 5 Hz stimulation increased cFos expression within LC neurons in stimulated LC hemispheres of ChR2+, but not in ChR2- animals 45 min (one-way ANOVA with Tukey's post hoc tests; F(3, 14) = 12.91, p = 0.000256) and 90 min after stimulation onset (one way ANOVA with Tukey's post hoc tests; F(3, 14) = 5.866, p = 0.00824). ChR2- (45 min), n = 5; ChR2- (90 min), n = 5; ChR2+ (45 min), n = 4; ChR2+ (90 min), n = 4. Scale bar: 100µm. **k**, Quantification of cortical MHPG/NA ratio, as measured by uHPLC, after 5 Hz optogenetic LC activation in ChR2- and ChR2+ animals. 5 Hz stimulation increased cortical NA turnover in ChR2+ animals (unpaired t test; 45 min: t(3.6) = 8.444, p = 0.001681; 90 min: t(4.0854) =3.4127, p = 0.02608). ChR2- 45min, n = 5; ChR2- 90min, n = 5; ChR2+ 45min, n = 6; ChR2+ 90min, n = 5. **l**, Average pupil size changes in response to 5 Hz optogenetic LC activation in ChR2- and ChR2+ animals. 5 Hz stimulation increased pupil size in ChR2+, but not ChR2- animals. **m**, Volcano plots showing differentially-expressed RNA transcripts between ChR2- and ChR2+ animals 45 and 90 min after 5 Hz optogenetic LC activation in the ventral (vHC) hippocampus. Red and blue values represent changes with FDR-adjusted p<0.05 (ChR2- n = 10, ChR2+ n = 11). **n**, Heatmap showing genes that are commonly differentially expressed by yohimbine, chemogenetic and optogenetic induced LC activation. **o**, Logarithmic cumulative rank of genes across all experiments from figure 1 and 2 in terms of their NA responsiveness. A lower cumulative rank indicates that a gene is among the more significant hits across all analyses (for full list of included analyses see methods). Labels indicate the 10 genes identified to be most responsive to LC-NA stimulation. *p < 0.05, **p < 0.01, ***p < 0.001, ****p < 0.0001.

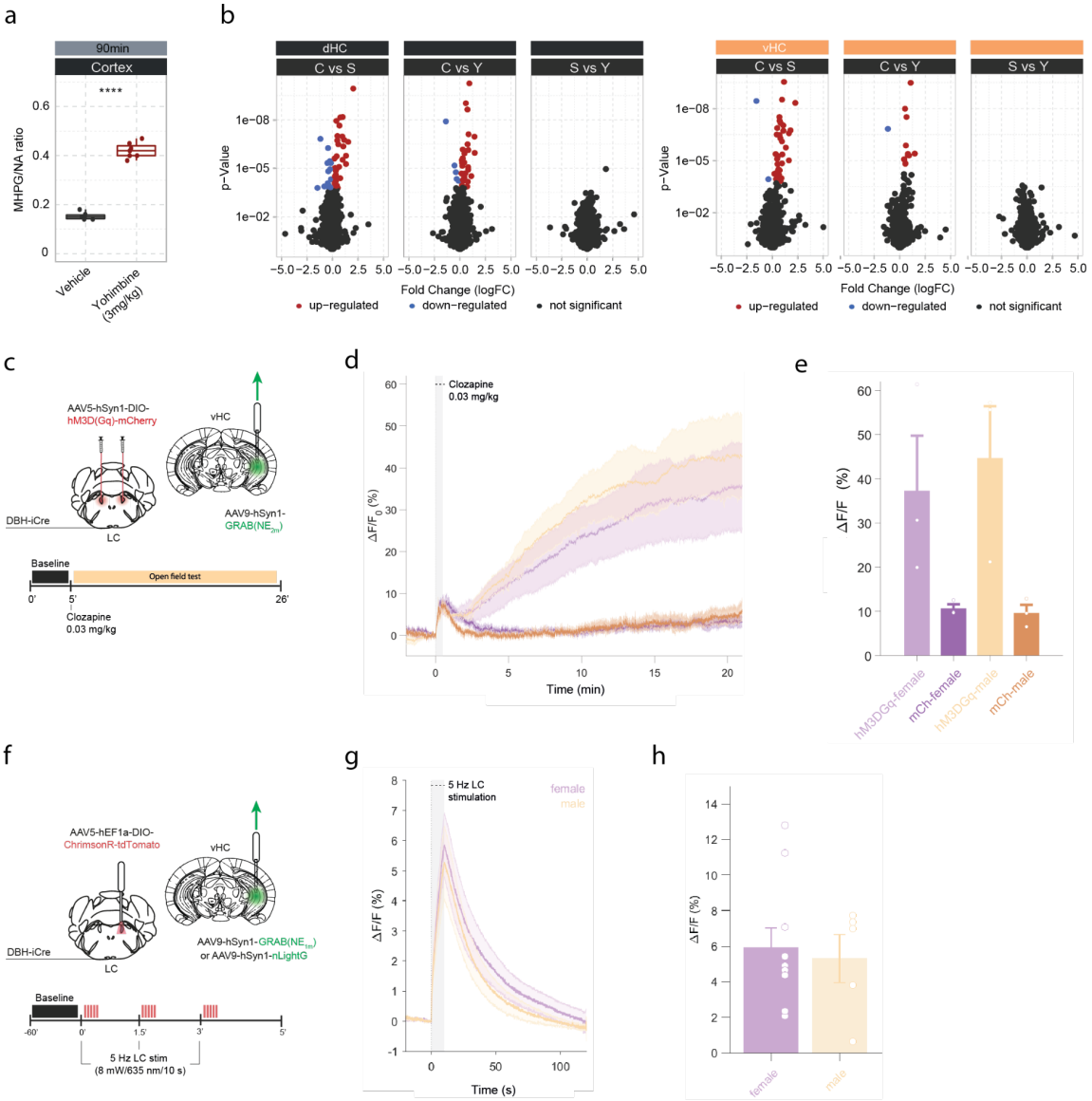

Supplementary Figure 2. Yohimbine-induced changes in NA turnover and gene expression, and validation of opto- and chemogenetic NA release in the hippocampus. a, Quantification of cortical MHPG/NA ratio, as measured by uHPLC, 90 min after systemic injection of vehicle or yohimbine (3 mg/kg, i.p.). Yohimbine increases cortical NA turnover (unpaired *t* test; t(8.9) = -20.099, p = 1.015e-08). Vehicle, n = 6; Yohimbine , n = 7. **b**, Volcano plots showing differentially expressed RNA transcripts between control (C) and acute stress (S) or yohimbine (Yoh) injected animals 45 min after stress or yohimbine injection in the dorsal (dHC) and ventral (vHC) hippocampus, as well as a direct comparison between the two responses. Red and blue values represent changes with FDR-adjusted p<0.05 (Veh n = 5, Yoh n = 5). ****p < 0.0001. **c**, Schematic of fiber photometry recording of hippocampal NA during chemogenetic activation of the LC. After 5 min of baseline recording in the homecage animals were injected with clozapine (0.03mg/kg, i.p.) and placed in the OFT for 21min. **d**, Average ΔF/F traces of $GRAB_{NE2m}$ photometry recordings in response to chemogenetic activation of the LC (mean±SEM for hM3DGq+ and hM3DGq- split into females and males, n=3/group/sex). **e**, Peak ΔF/F response of fiber photometry trace. **f**, Schematic of fiber photometry recording of hippocampal NA during optogenetic activation of the LC. Animals were lightly anesthetized (1.5% isoflurane) and recorded in a stereotaxic frame. After 1 min baseline recording, animals were stimulated three times with 5Hz for 10s (10ms pulse width, ~8mW laser power) and recorded for 2 min post-stimulation. **g**, Average ΔF/F traces of the NA sensors $GRAB_{NE1m}$ and nLightG in response to optogenetic activation of the LC (mean±SEM for females and males, n(females)= 10, n(males)=5. **h**, Peak ΔF/F response of fiber photometry traces.

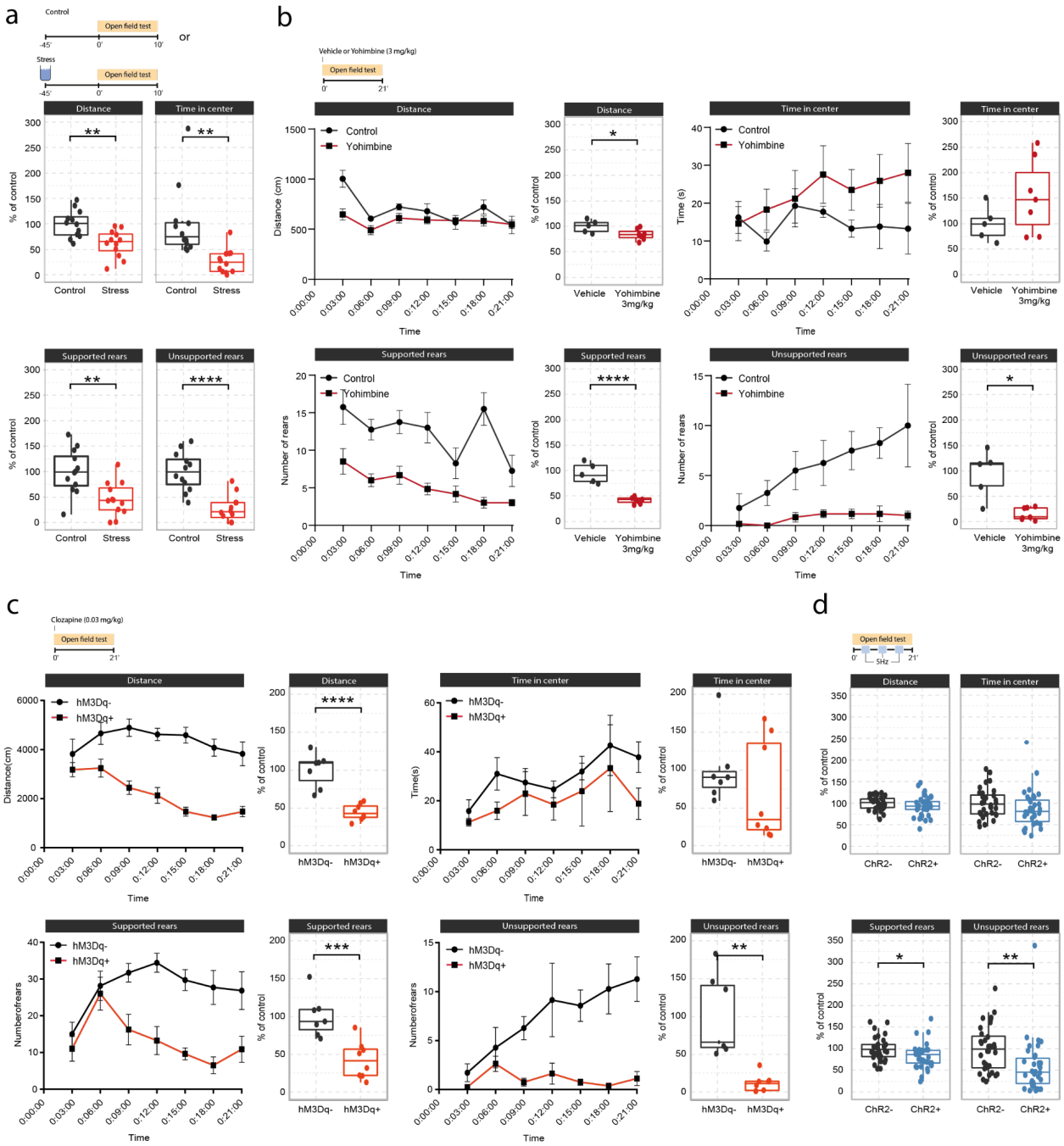

Supplementary Figure 3. Effects of acute stress and noradrenergic stimulation on anxiety-like behavior in the open field test. a, Stress-induced changes in the open field test 45 min after stress onset. Stressed animals show overall reductions in distance traveled (unpaired t-test; t=3.55, df=22, *p*=0.0018), time in center (welch unpaired t-test; t=3.50, df=13.61, *p*=0.0036), supported rears (unpaired t-test; t=3.39, df=22, *p*=0.0026) and unsupported rears (unpaired t-test; t=5.53, df=22, *p* = 1.47e-05) compared to controls (Control *n* = 12; Stress *n* = 12). This data have been previously published (von Ziegler et al. 2022). **b**, Yohimbine (3 mg/kg, i.p.) injected animals show reduced distance traveled (unpaired t-test; t=2.39, df=10, *p*=0.03772), reduced supported rears (unpaired t-test; t=6.56, df=10, *p*=0.00006) and reduced unsupported rears (welch unpaired t-test; t=3.69, df=4.4, *p* = 0.01785) compared to vehicle injected animals (Vehicle *n* = 6; Yohimbine *n* = 7). **c**, Chemogenetic LC activation induced changes in the open field test immediately after clozapine (0.03 mg/kg, i.p.) injection. hM3Dq+ animals show reduced distance traveled (unpaired

t-test; t=6.28, df=13, p=0.00003), reduced supported rears (unpaired t-test; t=4.28, df=13, p=0.0009), as well as reduced unsupported rears (welch unpaired t-test; t=4.28, df=13, p = 0.00437) compared to hM3D- animals (hM3Dq- n = 7; hM3Dq+ n = 8). **d**, Optogenetic 5 Hz LC activation induced changes during the open field test. ChR2+ animals show reduced supported rears (unpaired t-test; t=2.42, df=64, p=0.0185) and reduced unsupported rears (unpaired t-test; t=2.91, df=64, p = 0.00499) compared to ChR2- animals (ChR2- n = 32; ChR2+ n = 36). Data expressed as mean ± SEM. *$p < 0.05$, **$p < 0.01$, ***$p < 0.001$, ****$p < 0.0001$.

a

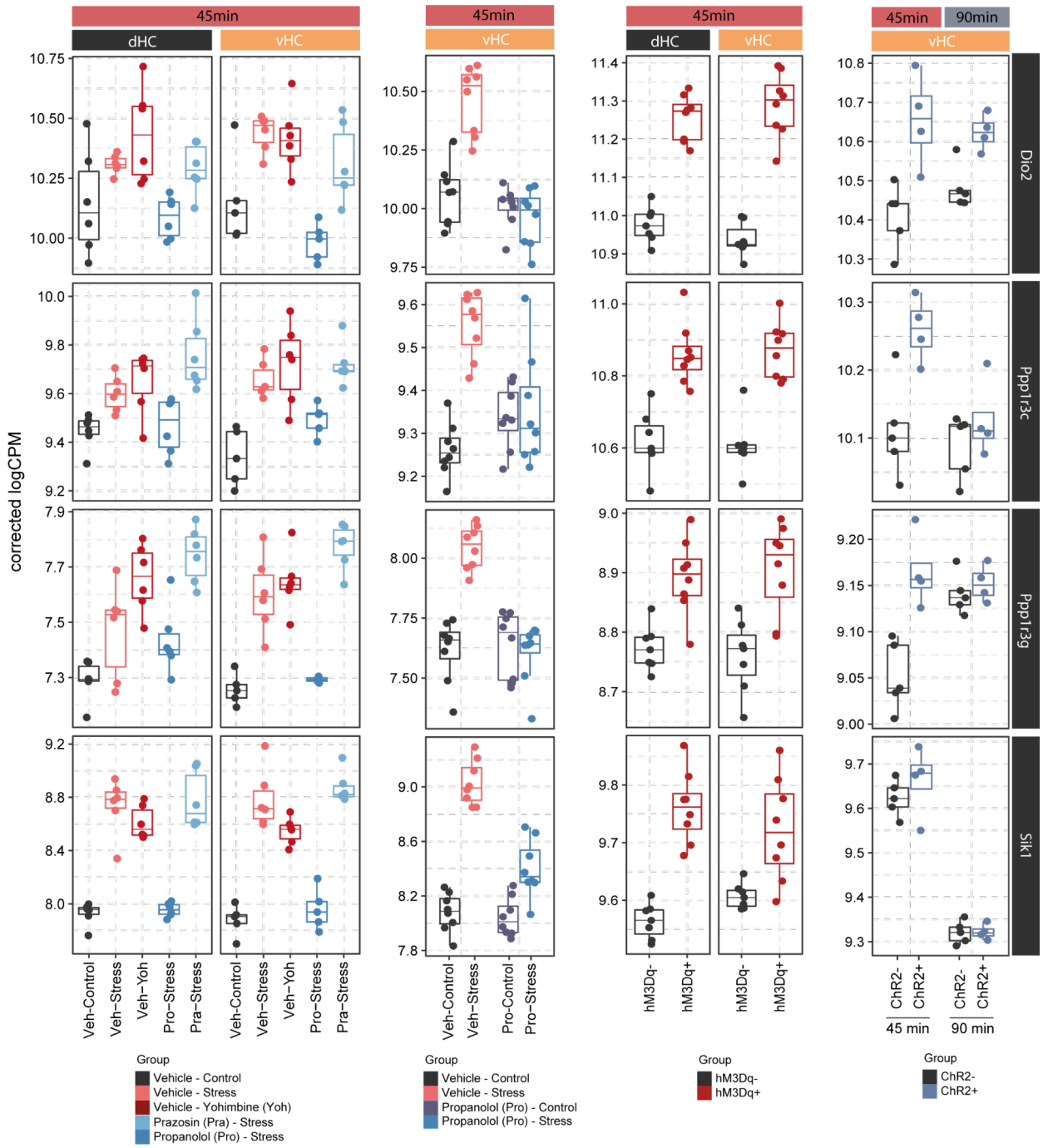

Supplementary Figure 4. Expression of *Dio2*, *Ppp1r3c*, *Ppp1r3g* and *Sik1* is consistent across pharmacological, chemogenetic and optogenetic manipulations of the noradrenergic system. a, Selective boxplots showing the expression changes of top 4 most responsive genes across all LC-NA manipulations. *Dio2, Ppp1r3c, Ppp1r3g and Sik1* are plotted across experiments in response to acute swim stress exposure, yohimbine (3 mg/kg, i.p.), swim stress and propranolol (10 mg/kg, i.p.), swim stress and prazosin (1 mg/kg, i.p.), as well as chemogenetic and optogenetic LC activation.

Our optogenetic data have demonstrated that LC neurons engage transcriptomic responses when firing at 5 Hz. Recent work has suggested that the effects of LC stimulation on brain processes, from behavior to brain network activity, depend on the firing pattern and frequency of the LC (Harley and Yuan 2021; Ghosh et al. 2021; Grimm et al. 2022). To investigate if the molecular responses would differ between these stimulation conditions, we optogenetically activated the LC using two tonic paradigms (3 and 5 Hz), and one phasic paradigm (15 Hz, see schematic in Fig. 3a). Stimulation was again conducted unilaterally in a 3 min off/on paradigm for 21 minutes for each of the stimulation groups, and tissue was collected for RNA-sequencing 45 min after stimulation onset (Fig. 3a). To increase statistical power in the face of higher variability due to the relatively small sample sizes (n=5-6 mice per group), we restricted our analysis to the ten most LC-NA-responsive genes identified earlier. Surprisingly, we found that expression of these genes was similarly affected by tonic 3 Hz, 5 Hz and phasic 15 Hz LC stimulation (Fig 3b). These findings suggest that in contrast to circuit-wide changes, the molecular consequences to NA release are independent of the firing intensity and activity pattern of the LC neurons. While these transcriptomic changes seem to depend on LC-NA activity, our approach so far was not able to resolve whether NA mediates gene expression via direct effects within the hippocampus. Specifically, due to the widespread projections of the LC, it is possible that activation of other brain regions or other neurotransmitter systems might have led to indirect regulation of gene expression in the hippocampus. Thus, we selectively targeted only a subpopulation of LC neurons projecting to the hippocampus (LC_{HC}) using a unilateral, retrograde optogenetic approach (Fig. 3c). Retrograde virus expression was restricted to dorsomedially located LC neurons ipsilateral to the injection site (Fig. 3d), as previously described (Robertson et al. 2013). To confirm successful LC_{HC} stimulation, we directly assessed NA turnover in the cortex and dHC. Indeed, 5Hz stimulation of LC_{HC} neurons led to an increased MHPG/NA ratio 45 min after stimulation onset in the ipsilateral dHC but not in the cortex (Fig. 3e). In addition, 5 Hz stimulation of LC_{HC} neurons did not impact pupil size, emphasizing the modular organization of the LC (Fig. 3f). Within the vHC of the same animals we then assessed the transcriptional impact of targeted LC_{HC} 5 Hz activation on the top ten NA-sensitive genes in the vHC at the 45 min time point. Indeed, activation of hippocampus-projecting LC neurons affected most target genes, including *Dio2*, *Ppp1r3c* and *Ppp1r3g* (Fig. 3g-h).

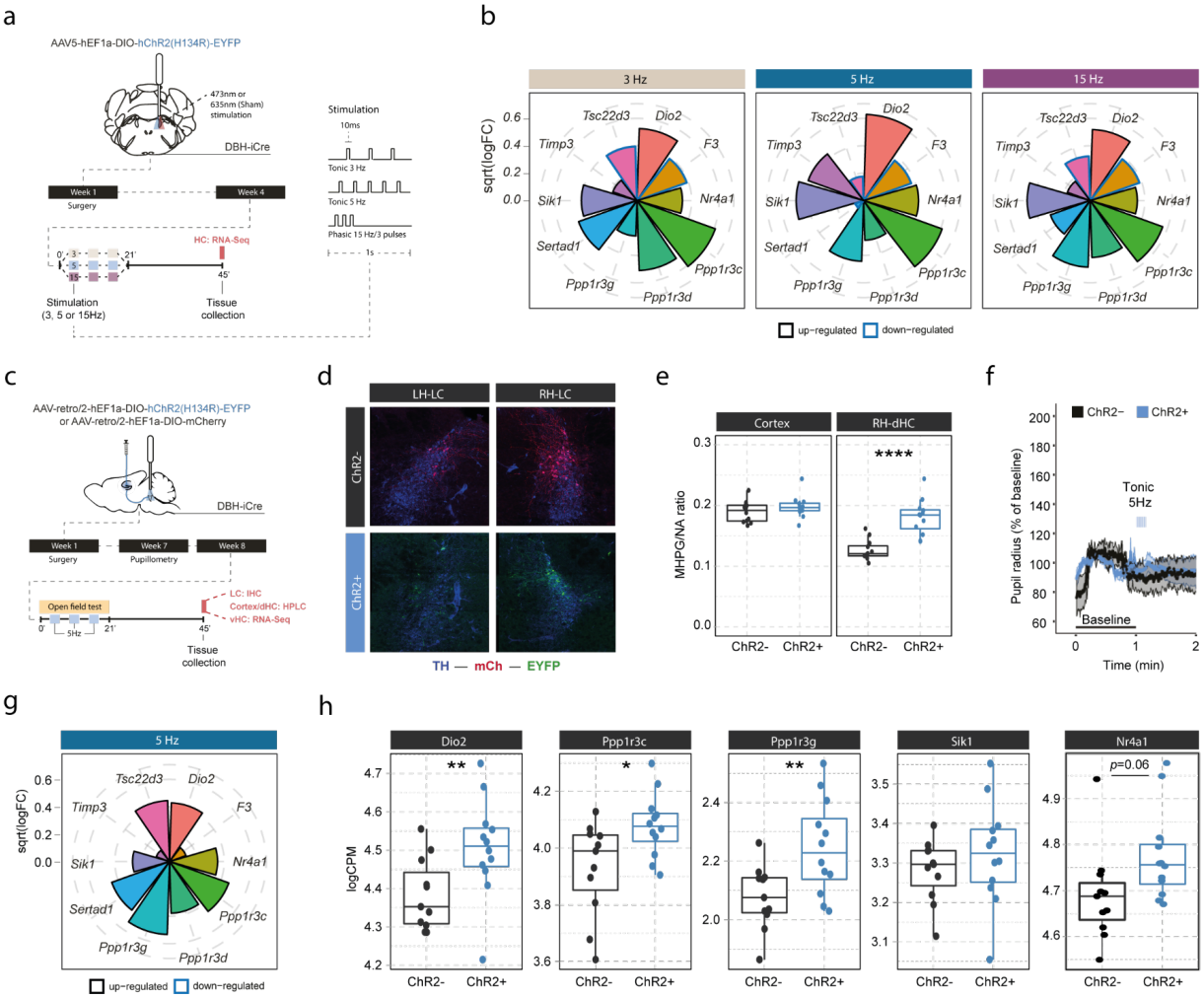

Fig. 3: LC-NA mediated molecular responses in the hippocampus are independent of LC firing pattern and frequency and are directly stimulated via hippocampus-projecting LC neurons. a, Experimental design for assessing molecular changes in the hippocampus induced by optogenetic LC activation with tonic (3 Hz and 5 Hz) and phasic (15 Hz) firing patterns. **b**, Radial plots showing expression changes (based on the logFC) of the most LC-NA-responsive genes after optogenetic LC activation in ChR2+ animals compared to controls (Sham $n = 6$, 3 Hz $n = 6$, 5 Hz $n = 7$, 15 Hz $n = 6$). Black borders indicate that the gene is upregulated, blue border downregulated. **c**, Experimental design for assessing molecular changes in the hippocampus induced by retrograde optogenetic 5 Hz activation of hippocampus projecting LC neurons (LC_{HC}). **d**, Representative images of retrograde mCherry (mCh, red) and ChR2-EYFP (EYFP, green) expression in tyrosine hydroxylase (TH, blue) positive LC neurons across hemispheres. **e**, Cortical and right dorsal hippocampal (RH-dHC) NA turnover as measured by ultra-high performance liquid chromatography 45 min after 5 Hz optogenetic activation of LC_{HC} neurons in ChR2- and ChR2+ animals. 5 Hz stimulation of LC_{HC} neurons increased dorsal hippocampal but not cortical NA turnover in ChR2+ animals (unpaired t test; t(17.43) = -5.5997, p = 2.911e-05). ChR2-, n = 12; ChR2+, n = 12. ****$p < 0.0001$. **f**, Average pupil size changes in response to 5 Hz optogenetic activation of LC_{HC} projecting neurons in ChR2- and ChR2+ animals. **g**, Radial plots showing expression changes (based on the logFC) of the top ten LC-NA responsive genes in response to optogenetic LC_{HC} activation with tonic 5 Hz stimulation in ChR2+ animals compared to ChR2- 45 min after stimulation onset (ChR2- $n = 12$, ChR2+ $n = 12$). **h**, Selective boxplots of NA-responsive genes *Dio2*, *Ppp1r3c*, *Ppp1r3g*, *Sik1* and *Nr4a1* in response to 5 Hz optogenetic activation of LC_{HC} projecting neurons in ChR2- and ChR2+ animals 45 min after stimulation onset. (ChR2- $n = 12$, ChR2+ $n = 12$). 5 Hz optogenetic activation of LC_{HC} projecting neurons increased hippocampal expression of *Dio2*, *Ppp1r3c*, *Ppp1r3g* and *Nr4a1*. *$p < 0.05$, **$p < 0.01$, ***$p < 0.001$, ****$p < 0.0001$.

To understand in more detail how these NA-sensitive genes are affected by different stressors, we investigated whether the expression of *Dio2, Ppp1r3c, Ppp1r3g, Sik1* and *Nr4a1* is specific to acute swim stress exposure or independent of the stress context. Therefore, we assessed their expression in a dataset comparing the effect of various stressors on the hippocampal transcriptome (Floriou-Servou et al. 2018). We found that these genes are not only upregulated by swim stress, but also by novelty stress, restraint and footshock stress (Fig. 4b). This suggests that expression of these genes is robustly induced by a wide range of stressors.

We then interrogated a recently published stress resource, which tracks stress-induced transcriptional changes over time in the hippocampus (von Ziegler et al. 2022). Across 4 hours following acute swim stress exposure, we found two distinctive expression patterns among these genes. While *Sik1* and *Nr4a1* show the characteristics of an immediate early gene with a sharp rise and fall in expression within 90 min of stress onset, upregulation of *Dio2, Ppp1r3c* and *Ppp1r3g* is maintained for at least 2-4 hours following stress exposure (Fig. 4d), suggesting that mechanisms are in place to prolong expression beyond the initial rise in NA. Reanalysis of a hippocampal single-nucleus RNA-sequencing dataset after a swim stress challenge (von Ziegler et al. 2022) revealed that stress-induced upregulation of *Dio2, Ppp1r3c* and *Ppp1r3g* seems predominantly restricted to astrocytes, while *Sik1* and *Nr4a1* show a broader expression among glia, neuronal and vascular cells.

Finally, to determine if these transcripts are also actively translated in astrocytes after stress exposure, we re-analyzed a dataset using translating ribosome affinity purification followed by RNA sequencing (TRAPseq) - in astrocytes of the somatosensory cortex after a similar acute swim stress paradigm as described here (Murphy-Royal et al. 2020). We found that *Dio2*, *Ppp1r3c, Ppp1r3g* and *Nr4a1* are significantly upregulated after stress exposure. Altogether, these results highlight that the NA-dependent gene expression changes that occur in response to stress exposures are most prominent in astrocytes.

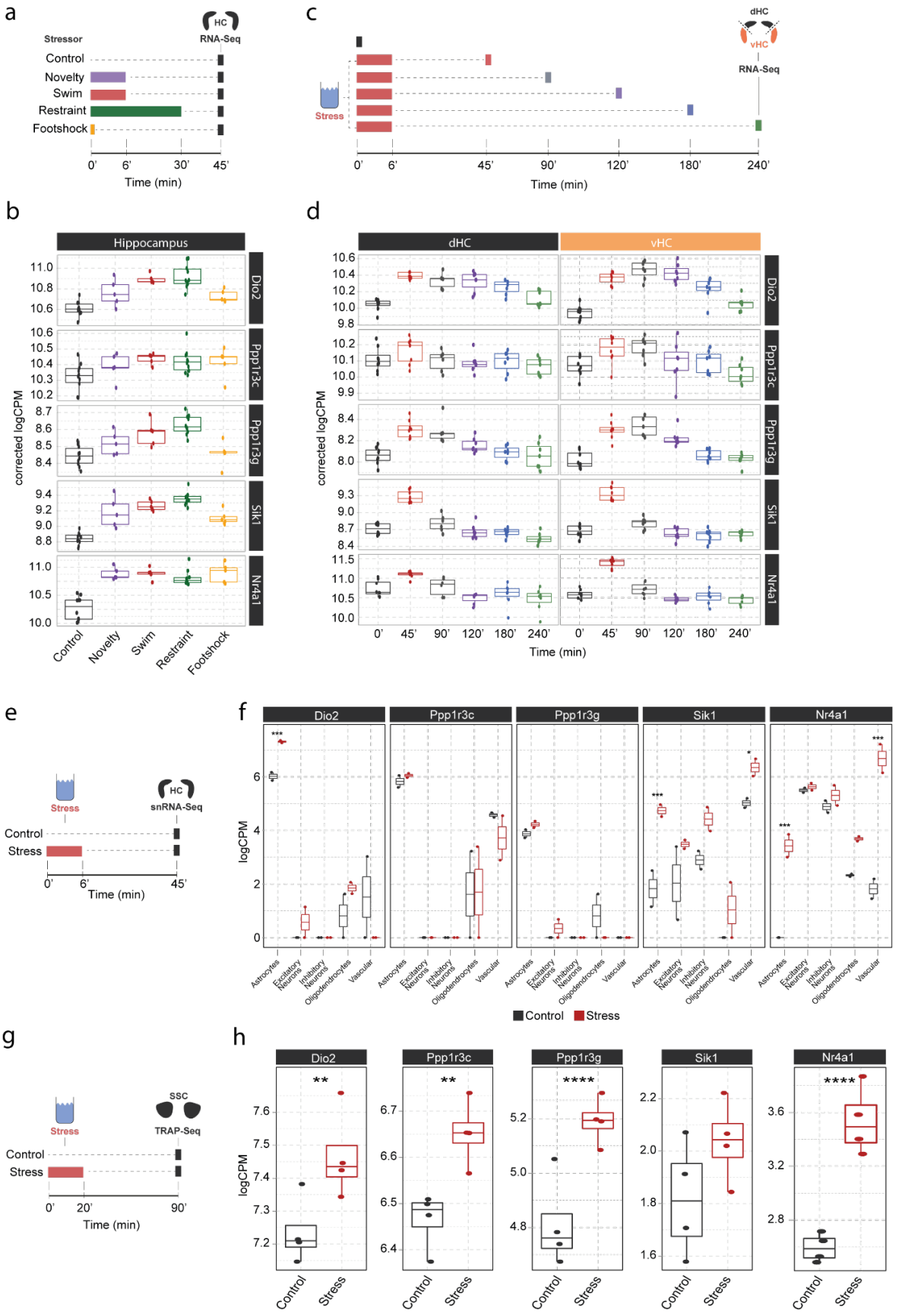
a
Stressor
HC
RNA-Seq
Control
Novelty
Swim
Restraint
Footshock
0'
6'
30'
45'
Time (min)
c
dHC
vHC
RNA-Seq
Stress
0'
6'
45'
90'
120'
180'
240'
Time (min)
b
Hippocampus
Dio2
Ppp1r3c
Ppp1r3g
Sik1
Nr4a1
corrected logCPM
Control
Novelty
Swim
Restraint
Footshock
d
dHC
vHC
Time (min)
e
Stress
HC
snRNA-Seq
Control
Stress
Time (min)
f
logCPM
Astrocytes
Excitatory Neurons
Inhibitory Neurons
Oligodendrocytes
Vascular
Control
Stress
g
Stress
SSC
TRAP-Seq
Control
Stress
Time (min)
h
logCPM
Control
Stress

Fig 4. Screening of publicly available datasets shows that the noradrenaline-regulated genes *Dio2, Ppp1r3c, Ppp1r3g, Sik1* and *Nr4a1* are induced by various stressors predominantly in astrocytes. a, Experimental design for assessing transcriptomic changes in the hippocampus induced by different stressors as performed by (Floriou-Servou et al. 2018). These stressors included a 10 min exposure to the open field test (Novelty), a 6 min cold swim stress (Swim), a 30 min immobilization stress (Restraint) and exposure to a 1 mA footshock (Footshock). **b**, Selective boxplots of top NA-responsive genes *Dio2*, *Ppp1r3c*, *Ppp1r3g*, *Sik1* and *Nr4a1* in response to different stressors. Control $n = 10$, Novelty $n = 5$, Swim $n = 5$, Restraint $n = 10$, Footshock $n = 5$. **c**, Experimental design for assessing transcriptomic changes in the dorsal and ventral hippocampus across 4 hours following acute swim stress exposure as performed by von Ziegler et. al . **d**, Selective boxplots showing expression changes of top NA-responsive genes *Dio2*, *Ppp1r3c*, *Ppp1r3g*, *Sik1* and *Nr4a1* across 4 hours following acute swim stress exposure. Control $n = 8$, 45 min $n = 8$, 90 min $n = 7$, 120 min $n = 7$, 180 min $n = 7$, 240 min $n = 7$. **e**, Experimental design for assessing single cell transcriptomic changes in the hippocampus 45 min following acute swim stress exposure by single-nucleus RNA sequencing as performed by von Ziegler et. al (von Ziegler et al. 2022). **f**, Selective boxplots showing expression changes of top NA-responsive genes *Dio2*, *Ppp1r3c*, *Ppp1r3g*, *Sik1* and *Nr4a1* across cell types of the hippocampus 45 min following acute swim stress exposure. Control $n = 2$, Stress $n = 2$. **g**, Experimental design for assessing actively translated RNA in the somatosensory cortex 90 min following a 20 min acute swim stress exposure by TRAP sequencing as performed by Murphy-Royal et. al (Murphy-Royal et al. 2020). **h**, Selective boxplots of top NA-responsive genes *Dio2*, *Ppp1r3c*, *Ppp1r3g*, *Sik1* and *Nr4a1* in the somatosensory cortex 90 min following a 20 min acute swim stress exposure. Acute stress increases the binding of *Dio2*, *Ppp1r3c*, *Ppp1r3g* and *Nr4a1* mRNA to the ribosome. Control $n = 4$, Stress $n = 4$. $^{*}p<0.05$, $^{**}p < 0.01$, $^{***}p < 0.001$, $^{****}p < 0.0001$.

Discussion

Dissecting stress with transcriptomics

The widespread molecular changes induced in the brain by an acute stress exposure (Stankiewicz et al. 2015; von Ziegler et al. 2022; Floriou-Servou et al. 2018; Mifsud et al. 2021) are part of a healthy stress response, and their dysregulation is often a hallmark of neuropsychiatric disorders (Girgenti, Pothula, and Newton 2021; Rubin, Gray, and McEwen 2014). To date, the contribution of corticosteroid signaling to stress-induced transcriptional changes has been well characterized (Mifsud et al. 2021; Gray et al. 2013; Meijer et al. 2022), yet the contribution of other stress-mediators remains unexplored. Here, we extensively characterize the contribution of noradrenergic signaling to the transcriptomic response in the hippocampus during stress. By combining transcriptomics with circuit-specific manipulation of the LC-NA system, our unbiased approach reveals a small, but highly reproducible set of genes that are regulated directly by NA release from the LC. This gene set identifies astrocytes as a key target for NA-induced transcriptional changes.

Complex interactions between stress mediators

Our results indicate that the transcriptomic response to a natural stressor is more complex than the gene expression changes induced solely by NA. This is well in line with the notion that multiple stress-mediators contribute to the molecular response, and that these systems can also interact with each other. The response to LC-NA activation we observe in our experiments is short in duration. Following temporally-precise optogenetic LC activation, gene expression changes did resolve within 90 min. This is noticeably different from an actual stress response, where gene expression evolves over a 4-hour period (von Ziegler et al. 2022). Specifically, LC-NA regulated genes like *Ppp1r3c, Ppp1r3g* and *Dio2*, were elevated for several hours after stress exposure (Fig. 4d). This suggests that other stress-induced signals can also regulate these genes more slowly or with a greater delay. Indeed, a recent study reported that activation of the glucocorticoid receptor by dexamethasone can induce strong transcriptomic changes 4 hours after injection across multiple brain regions (Gerstner et al. 2022). Analyzing their data we found that *Dio2*, *Ppp1r3c* and

Ppp1r3g were all upregulated 4 hours after dexamethasone injection. This supports the concept that NA can act as a rapid molecular regulator, whereas glucocorticoid signaling can extend these stress-induced changes over longer time periods (Hermans et al. 2014).
In contrast to the small set of genes triggered by isolated LC-NA activation, blocking β-receptors prevents the induction of a large fraction of genes normally activated by natural stressors. This suggests that even if NA release alone is not sufficient to activate large numbers of genes, it is required to enable or enhance gene expression triggered via other mechanisms. A powerful regulator of transcription is neuronal activity linked to enhanced glutamate release (Fernandez-Albert et al. 2019; Tyssowski et al. 2018). The notion that NA release could enhance glutamate-dependent transcriptional cascades is in line with physiological evidence that NA can increase the excitability of neurons (Bouret and Sara 2002), and with the "glutamate amplifies noradrenergic effects" (GANE) model, which posits that NA can amplify local glutamate release to create hot-spots of activity (Mather et al. 2016).
Finally, our observation that systemic administration of the α2-adrenergic receptor antagonist yohimbine very closely recapitulates the transcriptional response to stress stands in contrast to the much more selective transcriptional changes observed after chemogenetic or optogenetic LC-NA activation. This difference could be due to various factors. First, it remains unclear how strong the LC gets activated by yohimbine versus hM3Dq-DREADDs. However, given the potent LC activation observed after DREADD activation, it seems unlikely that yohimbine would lead to a more pronounced LC activation, thus explaining the stronger transcriptional effects. Second, contrary to LC-specific DREADD-activation, systemic yohimbine injection will also antagonize postsynaptic α2-adrenergic receptors throughout the brain (and periphery). More research is needed to determine whether this could have a more widespread impact on the hippocampus (and other brain regions) than isolated LC-NA activation, further enhancing excitability by preventing α2-mediated inhibition of cAMP production. Finally, systemic yohimbine administration and noradrenergic activity have been shown to induce corticosterone release into the blood (Johnston, Baldwin, and File 1988; Leibowitz et al. 1988; Fink 2016). Thus, yohimbine injection could have broader transcriptional consequences, including corticosteroid-mediated effects on gene expression.

Transcriptomic fingerprinting of NA effects using LC circuit manipulation

While systemic pharmacological treatments have been a common approach in studying the effects of different stress mediators and their receptors, they lack specificity and do not provide causal evidence that the release of a given stress mediator is sufficient to trigger molecular changes. By directly combining selective chemogenetic activation of the LC with transcriptomic analyses in the hippocampus, we were able to identify a subset of stress-responsive genes that depend on β-adrenergic signaling, and which can be triggered by NA alone in the absence of a physiological stress response. Using optogenetics we were able to validate these findings and further demonstrate that the strongest NA-mediated changes are similarly affected by tonic (3 Hz and 5 Hz) and phasic (15 Hz) LC stimulation. Interestingly, this is in contrast with our previous findings that these stimulation patterns differentially affect brain network connectivity (Grimm and Duss et al, 2022). This suggests that engagement of a transcriptomic response via β-adrenergic receptors seems common across these LC activity patterns, while changes on a network level might rely more on α1-mediated effects (Zerbi et al. 2019).
We found that direct activation of hippocampus-projecting LC neurons (LC_{HC}) was sufficient to increase expression of the top NA-sensitive target genes, suggesting that local NA release in the hippocampus is directly contributing to these changes during stress. While we did not extensively characterize LC_{HC} neurons, our data further show that in contrast to whole LC activation with 5 Hz, LC_{HC} neurons do not seem to project to the cortex, nor do they affect pupil size.

A uniform molecular response to stress and noradrenaline release in females and males

Our results, based on a meta-analysis of large sets of transcriptomic analyses across females and males, suggest that stress triggers a transcriptomic response in the hippocampus that is independent of sex.

Extensive analyses of male and female hippocampi in response to stress and propranolol also suggest that stress- and propranolol-sensitive genes show similar response profiles in both sexes. However, due to the multivariate design and our genome-wide approach, subtle changes might not have survived multiple-testing correction, particularly given that our study was not designed to track hormonal fluctuations across the estrous cycle, which is known to interact with noradrenaline signaling (Bangasser, Eck, and Ordoñes Sanchez 2019). An example is Ctla2b, which has previously been shown to be dependent on β-adrenergic signaling and to be selectively increased in females after stress exposure (Roszkowski et al. 2016). Indeed, targeted interrogation of our dataset confirms that Ctla2b is increased by stress only in females but not males, yet this effect fails to pass multiple testing correction (Supplementary Fig. 6). Ctla2b is also not included in the meta-analysis, as it did not pass the filtering step in our analysis pipeline due to very low baseline expression levels (see Methods). We provide a full list of genes that do not pass multiple testing correction, but still show nominally significant differences in gene expression (Supplementary Table 2). Although these changes must be treated with caution, our data allow targeted hypothesis testing of individual genes to generate leads for follow-up work.

Genes regulated by the LC-NA system

Across experiments, our transcriptomic screening revealed a conserved set of genes (Fig. 2o, Supplementary Table 1) that are selectively regulated by NA from LC projections in the hippocampus following acute stress exposure. Cross-referencing our data with publicly available single-cell databases suggests that - among the top ten LC-NA sensitive genes - most are enriched in astrocytes (Endo et al. 2022; von Ziegler et al. 2022). Interestingly, immediate early genes commonly upregulated during stress and associated with neuronal activation like *Fos*, *Egr1*, *Arc*, *Dusp1* and *Npas4* (Smith et al. 1992; Benito and Barco 2015; Fernandez-Albert et al. 2019; Tyssowski et al. 2018), are not upregulated by LC stimulation (Supplementary Fig. 5). Taken together, our findings further add to accumulating evidence highlighting astrocytes as a direct and major cellular target of the LC-NA system (Zenger et al. 2017; O'Donnell, Ding, and Nedergaard 2015; Dienel 2017).

Within the hippocampus, astrocytic pathways are emerging as important players for learning and memory processes (Gibbs, Hutchinson, and Hertz 2008; Bohmbach et al. 2022). In fact, it is well-known that NA enhances memory consolidation (Schwabe et al. 2022; McGaugh and Roozendaal 2002), and recent work suggests that these effects are mediated by astrocytic β-adrenergic receptors (Gao et al. 2016; Iqbal et al. 2023). Our transcriptomic screens revealed *Dio2* as the most prominent target influenced by LC activity. *Dio2* is selectively expressed in astrocytes and encodes for the intracellular type II iodothyronine deiodinase, which converts thyroxine (T4) to the bioactive thyroid hormone 3,3',5-triiodothyronine (T3) and therefore regulates the local availability of T3 in the brain (Bianco et al. 2019). Enzymatic activity of DIO2 has further been shown to be increased by prolonged noradrenergic transmission through desipramine treatment in LC projection areas (Campos-Barros et al. 1994). This suggests that the LC-NA system and its widespread projections could act as a major regulator of brain-derived T3. Notably, T3-signaling plays a role in hippocampal memory formation (Rivas and Naranjo 2007; Sui et al. 2006), raising the possibility that NA-induced *Dio2* activity in astrocytes might mediate some of these effects. Our molecular screening approach also revealed that three subunits of the astrocytic protein phosphatase 1 (*Ppp1r3d*, *Ppp1r3g* and *Ppp1r3c*) respond strongly to LC-NA activity. All three subunits enhance protein phosphatase 1 mediated glycogen synthesis. Especially *Ppp1r3c* expression has been found to be a master regulator of astrocytic glycogen synthesis and has previously been linked to NA activity (Allaman, Pellerin, and Magistretti 2000; Petit et al. 2021). Another important mechanism might include regulating sodium homeostasis via the widely expressed salt-inducible kinase 1 (*Sik1*). SIK1 has been shown to respond to neuronal activity and regulate Na+/K+-ATPase activity (Jaitovich and Bertorello 2010; Huang, White, and Leenen 2012; Feldman et al. 2000; Bertorello and Zhu 2009). It was also found to detect low glucose availability and initiate gluconeogenesis in liver cells (Wang et al. 2020), a process which could also be important for noradrenergic activity in the brain. Our findings support the idea of the LC-NA system as a major regulator of brain-wide

energy metabolism, stimulating astrocytic glycogen breakdown and consequently increasing energy supply to target areas (Coggan et al. 2018; Dienel 2017).

Another interesting molecular target is the Nuclear Receptor Subfamily 4 Group A Member 1 (Nr4a1), a widely expressed transcription factor that could trigger broader downstream changes. Within astrocytes, Nr4a1 activity was found to reduce oxidative stress and inflammation (Xu et al. 2015; Popichak et al. 2018) and might further regulate blood brain barrier integrity (Pan et al. 2021; Paillasse and de Medina 2015). Our re-analysis of published data showed that *Dio2*, *Ppp1r3c*, *Ppp1r3g* and *Nr4a1* are actively translated in somatosensory cortical astrocytes following acute stress exposure. It remains to be tested whether protein levels, transcription factor activity or enzymatic activity of these genes are also altered in the hippocampus, and what this ultimately means mechanistically for stress-related NA signaling.

Summary

Overall, we provide the first genome-wide characterization of the molecular impact of NA release in vivo in the brain. The set of genes that are sensitive to NA release from the LC point to astrocytes as key molecular targets of NA during stress, and suggest that astrocytic processes involving glycogen and thyroid hormone metabolism could be key to the neuromodulatory effects of NA in the hippocampus.

a

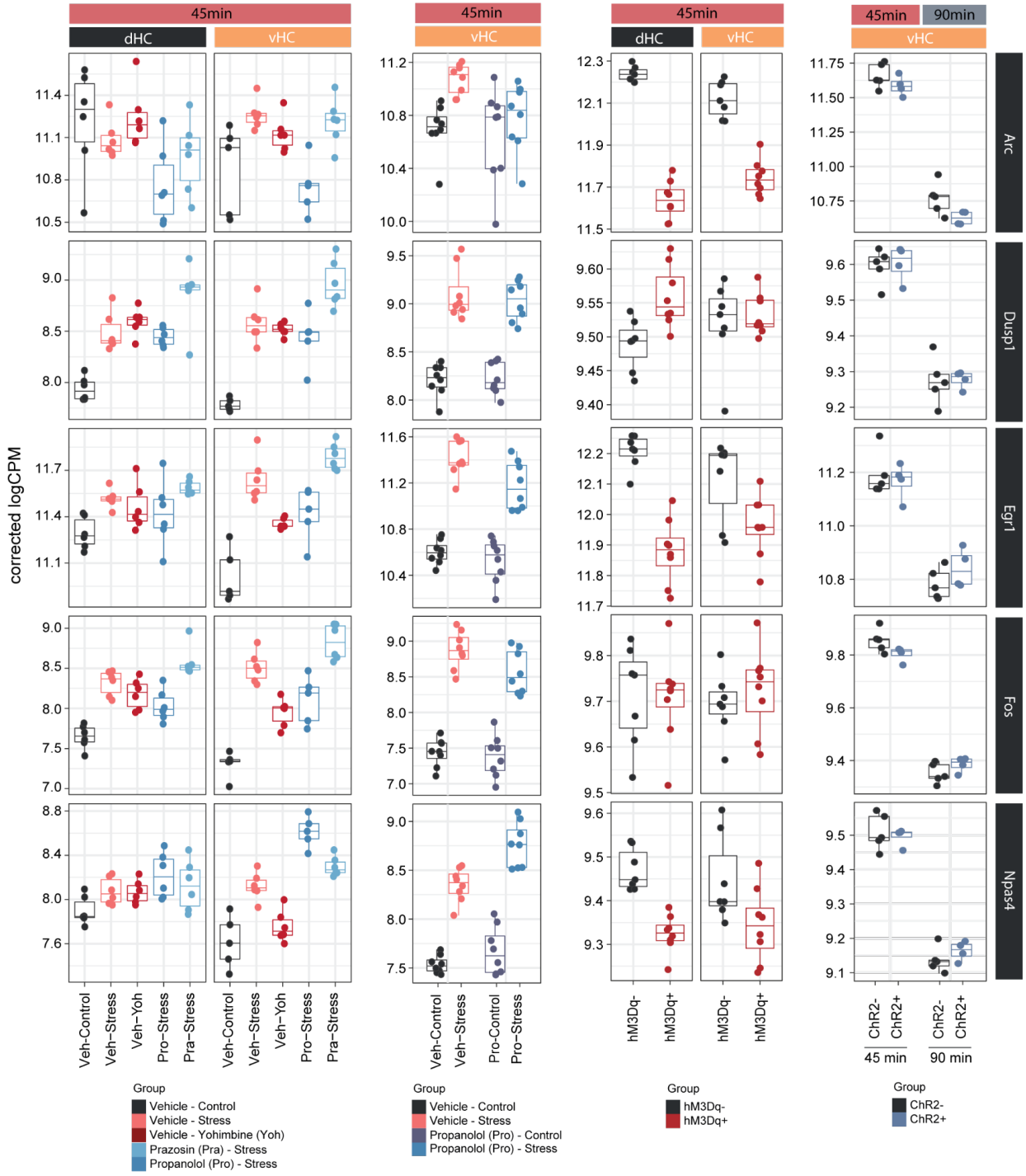

Supplementary Figure 5. Neuronal immediate early genes in the hippocampus are not regulated by noradrenaline signaling. **a**, Selective boxplots showing the expression changes of genes associated with neuronal activation (*Arc, Dusp1, Egr1, Fos* and *Npas4*) across experiments in response to acute stress and noradrenergic manipulation. Propranolol was not able to block the stress-induced expression of these genes, and locus coeruleus stimulation was not able to mimic their stress-induced upregulation.

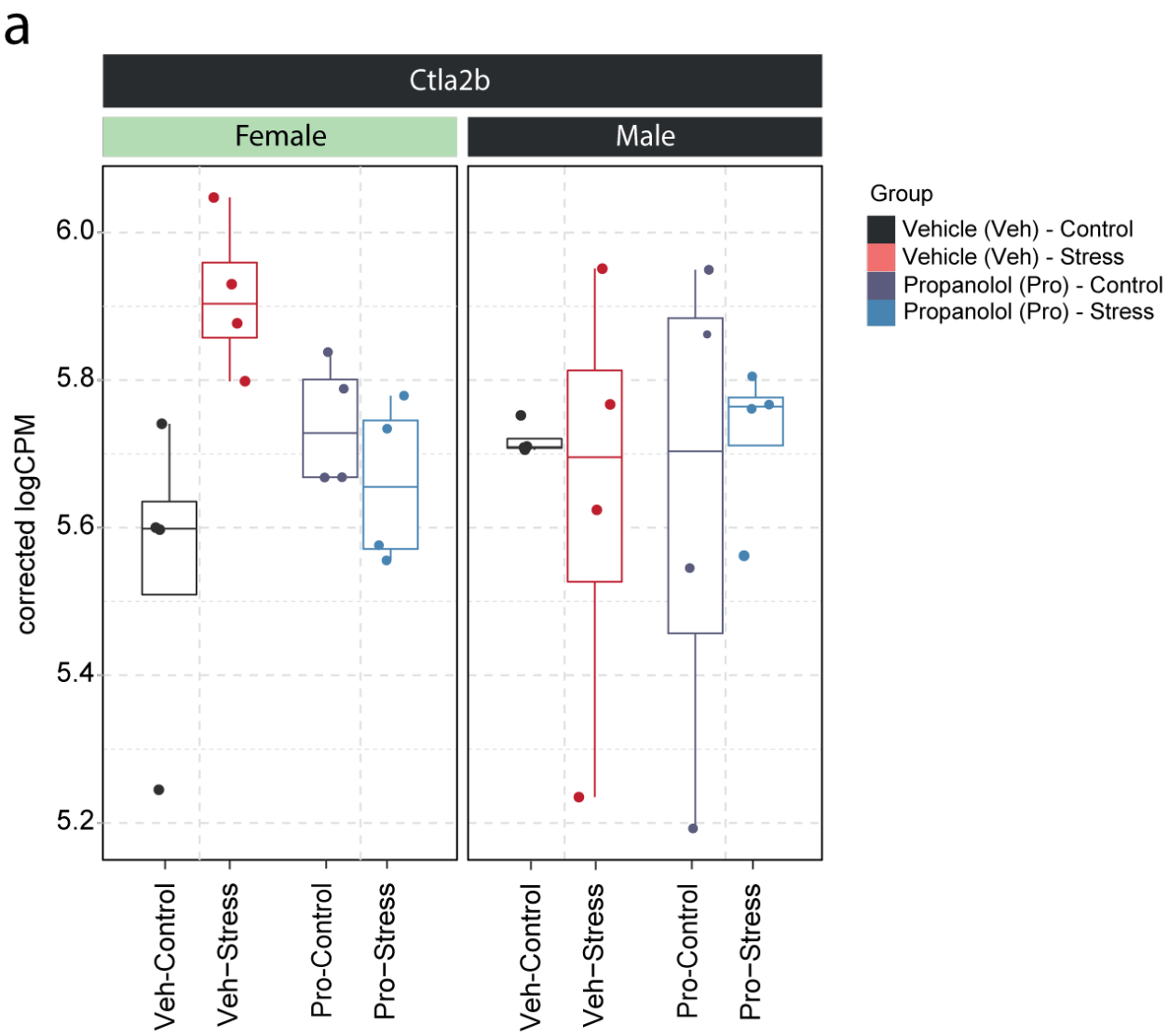

Supplementary Figure 6. Sex dependent expression of Ctla2b in the ventral hippocampus of female and male mice. a, Selective boxplot of *Ctla2b* expression - from data shown in figure 1g-h - in response to acute swim stress and propranolol 45 min after stress onset in female and male mice. $n = 4$ per group.

Supplementary Table 1. List of reproducible gene expression changes across various manipulations of the LC-NA system. This table displays the logarithmic cumulative rank of genes across all experiments from figures 1 and 2 in terms of their responsiveness to manipulatios of the LC-NA system. A lower cumulative rank indicates that a gene is among the more significant hits across all analyses (for full list of included analyses see methods). The top 10 genes from this list are shown in Figure 2o.

Supplementary Table 2. Sex-specific regulation of transcription in the ventral hippocampus after swim stress exposure. Differential expression analysis results for a sex:stress interaction performed across the meta-analysis of vHC datasets 45min after stress initiation (total of 50 males and 20 females). The table merges the results of both the edgeR and the DESeq2 analyses. Detailed information is provided in the sheet "ColumnDefinitions".

Methods

Animals

All experiments were conducted in accordance with the Swiss federal guidelines for the use of animals in research and under licenses ZH161/17, ZH106/20 and ZH067/2022 approved by the Zurich Cantonal veterinary office. For experiments with wild type animals, 2-3 month old C57Bl/6J mice were obtained directly from Janvier (France). For experiments involving chemo- and optogenetic LC manipulations, heterozygous C57BL/6-Tg(Dbh-icre)1Gsc mice were kept in breeding trios with wild-type C57BL/6J mice at the ETH Zurich animal facility (EPIC). All mice were housed in groups of 2-5 per cage in a temperature- and humidity-controlled facility on a 12-hour reversed light-dark cycle (lights off: 9:15 am; lights on: 9:15 pm), with food and water *ad libitum*, and used for experiments at the age of 2-4 months. All experiments were conducted during the animals' active (dark) phase. For all experiments, mice were single-housed 24 hours before exposure to stress or LC activation, which reduces corticosterone levels in both sexes, and avoids confounding gene expression effects from social stressors (Roszkowski et al. 2016; Bohacek et al. 2015).

Stereotactic Surgeries

For experiments involving hippocampal infusions, female C57BL/6-Tg(Dbh-icre)1Gsc mice at the age of 2-3 months were subjected to stereotactic surgery. The mice were anesthetized with 4% isoflurane and then placed in a stereotaxic frame with continuous anesthesia of 2% isoflurane. For analgesia, animals received a subcutaneous injection of 5 mg/kg Meloxicam and buprenorphine (0.1 mg/kg), as well as application of the local analgesics lidocaine (2 mg/kg) and bupivacaine (2 mg/kg) before and after surgery. After the skull was exposed, bregma (defined as the intersection of the coronal and sagittal suture) was located and the skull placement corrected for tilt and scaling. Bilateral holes were drilled above the hippocampus at -1.8 mm AP and +/- 1.5 mm ML from bregma, followed by the implantation of a bilateral guide cannula (62036, RWD Life Science, China) into the hippocampus (coordinates from bregma: -1.8 mm AP, +/- 1.5 mm ML, -1.5 mm DV).

For chemo- and optogenetic experiments male C57BL/6-Tg(Dbh-icre)1Gsc mice at the age of 2-3 months were subjected to stereotactic surgery. The mice were anesthetized with 4% isoflurane and then placed in a stereotaxic frame with continuous anesthesia of 2% isoflurane. For analgesia, animals received a subcutaneous injection of 5 mg/kg Meloxicam and a local anesthetic (Emla cream; 5% lidocaine, 5% prilocaine) before and after surgery. After the skull was exposed, bregma was located and the skull placement corrected for tilt and scaling. Bilateral (chemogenetics) or unilateral (Right hemisphere, optogenetics) small holes were drilled above the LC at -5.4 mm AP and 0.9 mm ML from bregma. A pneumatic injector (Narishige, IM-11-2) and calibrated microcapillaries (Sigma-Aldrich, P0549) were then used to inject 1 µL of virus to the LC (coordinates from bregma: −5.4 mm AP, ± 1.0 mm ML, −3.8 mm DV). All Viral vectors were obtained from the Viral Vector Facility (VVF) of the Neuroscience Center Zurich. For chemogenetic experiments, either ssAAV-5/2-hSyn1-dlox-hM3D(Gq)_mCherry(rev)-dlox-WPRE-hGHp(A) (hM3Dq+) or ssAAV-5/2-hSyn1-dlox-mCherry(rev)-dlox-WPRE-hGHp(A) (hM3Dq-) were injected bilaterally for all experiments except fiber photometry recordings where animals were injected unilaterally.

For optogenetic experiments, ssAAV-5/2-hEF1α-dlox-hChR2(H134R)_EYFP(rev)-dlox-WPRE-hGHp(A) (ChR2+) or ssAAV-5/2-hEF1a-dloxEGFP(rev)-dlox-WPRE-bGHp(A) (ChR2-) were delivered unilaterally to the right hemisphere locus coeruleus. For retrograde activation of hippocampus projecting LC neurons, animals received one injection of either ssAAV-retro/2-hEF1a-dlox-hChR2(H134R)_EYFP(rev)-dlox-WPRE-hGHp(A) (ChR2+) or ssAAV-retro/2-hEF1a-dlox-mCherry(rev)-dlox-WPRE-hGHp(A) (ChR2-) to the ipsilateral dHC (coordinates from bregma: -2.10 mm AP, 1.5 mm ML; -1.8 mm DV) and vHC (coordinates from bregma: -3.30 mm AP, 2.75 mm ML; -4.0 mm DV). Additionally, all optogenetic animals were

unilaterally implanted with an optic fiber (200 µm diameter, 0.22 NA) above the LC (coordinates from bregma: -5.4 mm AP, 0.9 mm ML, -3.5 mm DV). For fiber photometry recordings, animals were injected with the optogenetic actuator ChrimsonR (ssAAV-5/2-hEF1α/hTLV1-dlox-ChrimsonR_ tdTomato(rev)-dlox-WPRE-bGHp(A); 4.7x10E12 vg/ml). Additionally, animals for both optogenetic and chemogenetic fiber photometry recordings received a second injection of a genetically encoded NA sensor (ssAAV-9/2-hSyn1-GRAB(NE1m)-WPRE-hGHp(A); 5.5x10E12 vg/ml, ssAAV-9/2-hSyn1- chI-nLightG-WPRE-bGHp(A); 5.5x10E12, or ssAAV-9/2-hSyn1-GRAB(NE2m)-WPRE-hGHp(A); 0.5x10E12 vg/ml) into the ipsilateral vHC (coordinates: AP -3.2 mm, ML -3.3 mm, DV -3.8 mm). To record from the vHC, an optic fiber was implanted 200 µm above the injection site (200 µm, NA=0.37; Neurophotometrics, USA). The health of all animals was monitored over the course of 3 consecutive days post-surgery. Experiments on operated animals were conducted 4-8 weeks post-surgery to allow for recovery and sufficient virus expression. All viruses were obtained from the Viral Vector Facility of the University of Zurich and ETH Zurich.

Drug injections/infusions

All drugs were freshly prepared immediately before experiments and dissolved in phosphate-buffered 0.9% saline (Gibco, pH 7.4). Drugs were administered intraperitoneally at their corresponding dosages: Yohimbine-Hydrochloride (3 mg/kg, Merck, Germany), Propranolol-Hydrochloride (10 mg/kg, Merck, Germany), Prazosin-Hydrochloride (1 mg/kg, Merck, Germany) and Clozapine (0.03mg/kg, Merck, Germany).

For intra-hippocampal infusions of isoproterenol hydrochloride (Merck, Germany), animals were restrained and the guide cannula was inserted with an injector needle (62236, RWD Life Science, China) connected to an infusion pump (R462 Syringe Pump, RWD Life Science, China) via plastic tubing. Prior to attachment, the tubing was filled with sunflower seed oil (Merck, Germany) and vehicle (0.9% saline) or isoproterenol, separated by a small air bubble. Afterwards, animals were allowed to freely roam their home cage for 2 minutes followed by bilateral intra-hippocampal infusions of vehicle drug or 1 µl of isoproterenol (3 µg/µl diluted in phosphate-buffered 0.9% saline) at 50 µl/min. Diffusion of vehicle and isoproterenol was allowed for another 2 min, before the animal was detached from the infusion setup and returned to its homecage.

Fiber photometry

Fiber photometry recordings were performed as previously reported (Grimm et al. 2022). In short, the green fluorescence signal from the NA sensors $GRAB_{NE1m}$, $GRAB_{NE2m}$, or nLightG were recorded using a commercially available photometry system (Neurophotometrics, Model FP3002) controlled via the open-source software Bonsai (2.6.2 version). Two LEDs were used to deliver interleaved excitation light: a 470 nm LED for recording NA-dependent fluorescent signal (F^{470}) and a 415 nm LED for NA – independent control signals (F^{415}). Recording rate was set at 60 Hz for both LEDs allowing 30 Hz per channel. Excitation power at the fiber tip (200 µm, 0.39 numerical aperture; Doric Lenses) was set to 25-35 µW. Recordings during optogenetic LC stimulation were performed during light anesthesia (1.5% isoflurane) while chemogenetic LC activation was recorded in awake, well-handled animals.

Forced swim test

For the forced cold swim stress, mice were placed for 6 min in a plastic beaker (20 cm diameter, 25 cm deep) filled with 18 ± 0.1°C water to 17 cm, in a room with dim red lighting. Immediately after stress exposure, mice returned to their assigned single-housing homecage.

Open field test (OFT)

Open-field testing was performed in a square 45 cm (l) × 45 cm (w) × 40 cm (h) arena, and consisted of four black Plexiglas walls and a white PVC floor. Mice were tested under dim lighting (5 lux at the center of the arena). Mice were placed directly into the center of the open field and the tracking/recording was initiated 2 seconds after the mouse was detected. The test lasted 10 min for acute stress exposed animals, 21 min

for yohimbine and optogenetic stimulated animals and 30 min for chemogenetic stimulated animals. Distance, time in center, supported and unsupported rearings were tracked by the software EthoVision XT14 (Noldus, Netherlands) and manual scoring. For pharmacological and chemogenetic experiments, animals received an i.p injection of yohimbine (3 mg/kg) or clozapine (0.03 mg/kg) immediately before being placed into the arena. For optogenetic experiments, animals were attached to the optic fiber and directly placed into the arena.

Optogenetic stimulation

Across optogenetic experiments the LC was stimulated with either 473 nm or 635 nm light at 10 mW power and 3 Hz, 5 Hz or 15 Hz frequency (10 ms pulse width) alternating between 3 min off and on as previously described (McCall et al. 2015; Grimm et al. 2022).

Pupillometry

Pupillometry was used to evaluate optogenetic LC stimulation as previously described (Privitera et al. 2020). At 3-4 weeks post-surgery, ChR2- and ChR2+ animals were anesthetized with 4% isoflurane and then placed in a stereotaxic frame with continuous anesthesia of 2% isoflurane. Recordings were performed of the right eye ipsilateral to the stimulated LC and consisted of an initial baseline recording of 60 seconds, followed by tonic LC stimulation (5 Hz at 10 mW for 10 s) and 1 min post stimulation recording. Pupil videos were tracked with DeepLabCut and analyzed with the Pupillometry App.

Tissue collection

At the appropriate time point after initiation of stress (for immediate groups within maximum 1 min after offset of stress) or LC activation, mice were euthanized by cervical dislocation and decapitation. The brain was quickly dissected on a cold glass plate and isolated hippocampi were separated by a cut at a ratio of 1:2 to divide the dHC and vHC. For experiments that were analyzed with uHPLC additionally the whole cortex was also collected. Isolated tissues were then snap-frozen in liquid nitrogen and stored at -80°C until further processing. For immunohistochemistry, the hindbrain (containing the LC) was isolated with a single cut from a razor blade at the beginning of the cerebellum and directly transferred to a tube with 4% paraformaldehyde solution. All tissue dissections were performed between 11am and 5pm during the dark phase of the 12-hour reversed light-dark cycle.

Immunohistochemistry

LC containing hindbrain samples were fixed for 2 hours in ice-cold paraformaldehyde solution (4% PFA in PBS, pH 7.4). The tissue then was rinsed with PBS and stored in a sucrose solution (30% sucrose in PBS) at 4°C, overnight. The tissue was frozen in tissue mounting medium (Tissue-Tek O.C.T Compound, Sakura Finetek Europe B.V., Netherlands), and sectioned coronally using a cryostat (Leica CM3050 S, Leica Biosystems Nussloch GmbH) into 40 µm thick sections. The sections were immediately transferred into ice-cold PBS. LC containing sections were stained in primary antibody solution with 0.05% Triton X-100, and 4% normal goat serum in PBS at 4C under continuous agitation over 2 nights. The primary antibodies used were: mouse anti-TH (22941, Immunostar, 1:1000), chicken anti-GFP (ab13970, Abcam, 1:1000) and rabbit anti-cFOS (226 003, Synaptic Systems, 1:5000). Afterwards, the sections were washed 3 times in PBS, and transferred to secondary antibody solution containing 0.05% Triton X-100, and 4% normal goat serum in PBS. The secondary antibodies used were: goat anti-mouse Alexa 488 (ab150113, Abcam, 1:300), goat anti-mouse Cy3 (115-165-003, Jackson ImmunoResearch, 1:300), goat anti-chicken Alexa 488 (A-11039, Thermo Fischer Scientific, 1:300), goat anti-rabbit Alexa 488 (A-11008 Thermo Fisher Scientific, 1:500), goat anti-rabbit Alexa 546 (A-11035, Thermo Fisher Scientific, 1:300) and donkey anti-mouse Alexa 647 (A-31571, Thermo Fisher Scientific, 1:300). Nissl was stained by NeuroTrace 640/660 Nissl stain (N21483, Thermo Fisher Scientific). After 3 more PBS washes, the sections were mounted onto glass slides (Menzel-Glaser SUPERFROST PLUS, Thermo Scientific), air-dried and coverslipped with Dako fluorescence mounting medium (Agilent Technologies). Microscopy images were acquired in a confocal laser-scanning

microscope (CLSM 880, Carl Zeiss AG, Germany) with a 20x objective. Images were analyzed using FIJI and for cFos quantification TH+ and cFos+ cells were counted manually.

Ultra-high performance liquid chromatography (uHPLC)

To quantify noradrenergic (NA; MHPG) compounds from cortical and hippocampal tissue, a reversed-phase uHPLC system coupled with electrochemical detection (RP-uHPLC-ECD) was used (Alexys™ Neurotransmitter Analyzer, Antec Leyden, Zoeterwoude, Netherlands). In short, our previously validated RP-HPLC method with ion pairing chromatography was applied as described (Van Dam et al., 2014), albeit with minor modifications regarding the installed column (BEH C18 Waters column, 150 mm x 1 mm, 1.7 µm particle size) and pump preference (LC110S pump, 470-480 bar; flow rate of 62 L/min), achieving the most optimal separation conditions in a RP-UHPLC setting. Brain samples were defrosted to 4°C and subsequently homogenized in 800-900 µL ice-cold sample buffer (50 mM citric acid, 50 mM phosphoric acid, 0.1 mM EDTA, 8 mM KCl and 1.8 mM octane-1-sulfonic acid sodium salt (OSA), adjusted to pH = 3.6), using a Precellys® Minilys Personal Tissue Homogenizer (Bertin Technologies™, France) with CK14 1.4 mm ceramic beads (40-60 sec approximately, full speed). To remove excess proteins, 450 mL homogenate was transferred onto a 10,000 Da Amicon Ultra 0.5 Centrifugal Filter (Millipore, Ireland) that had been pre-washed twice using 450 µL sample buffer (centrifugation: 14,000 x g, 20 min, 4°C). The Amicon filter loaded with the homogenate was then centrifuged (14,000 x g, 20 min, 4°C). Finally, the filtrate was transferred into a polypropylene vial (0.3 mL, Machery-Nagel GmbH & Co. KG, Germany) and automatically injected into the uHPLC column by the Alexys AS110 Autosampler (5 µL sample loop). Levels of the monoamines and metabolites were calculated using Clarity software™ (DataApex Ltd., v86.12.0.77208, 2015, Prague, Czech Republic).

RNA extraction

Dorsal and ventral hippocampal samples were homogenized in 500 µL Trizol (Invitrogen 15596026) in a tissue lyser bead mill (Qiagen, Germany) at 4°C for 2 mins, and RNA was extracted according to manufacturer's recommendations. This was followed by determining RNA purity and quantity with a UV/V spectrophotometer (Nanodrop 1000).

Bulk RNA sequencing and data analysis

For experiments shown in Figure 1c-e and 2, bulk mRNA sequencing was performed at the Functional Genomics Center Zurich (FGCZ) core facility. Data shown in figure 1c-e and 2c-d belong to the same experiment and were split up for better visualization of effects after sample processing and RNA sequencing analysis was performed. RNA integrity was assessed with high sensitivity RNA screen tape on an Agilent Tape Station/Bioanalyzer, according to the manufacturer’s protocol. The RIN values of all samples ranged from 8.4 to 10.0. For library preparation, the TruSeq stranded RNA kit (Illumina Inc.) was used according to the manufacturer’s protocol. For bulk sequencing library preparation, the TruSeq stranded RNA kit (Illumina Inc.) was used according to the manufacturer’s protocol. The mRNA was purified by polyA selection, chemically fragmented and transcribed into cDNA before adapter ligation. Single-end (100nt) sequencing was performed with HiSeq 4000. Samples within experiments were each run on one or multiple lanes and demultiplexed. A sequencing depth of ~20M reads per sample was used. Bulk mRNA sequencing for experiments shown in Figure 1g-h and 3 were performed at Novogene UK. Total RNA samples were used for library preparation using NEB Next® Ultra RNA Library Prep Kit for Illumina®. Indices were included to multiplex multiple samples. Briefly, mRNA was purified from total RNA using poly-T oligo-attached magnetic beads. After fragmentation, the first strand cDNA was synthesized using random hexamer primers followed by the second strand cDNA synthesis. The library was ready after end repair, A-tailing, adapter ligation, and size selection. After amplification and purification, insert size of the library was validated on an Agilent 2100 and quantified using quantitative PCR (Q-PCR). Libraries were then

sequenced on Illumina NovaSeq 6000 S4 flowcell with PE150 according to results from library quality control and expected data volume. Samples within experiments were each run on one or multiple lanes and demultiplexed. A sequencing depth of ~40M reads per sample was used.
For all experiments, adapters were trimmed using cutadapt (Martin 2011) with a maximum error rate of 0.05 and a minimum length of 15. Kallisto (v0.44.0) (Bray et al. 2016) was used for pseudo alignment of reads on the transcriptome level using the genecode.vM17 assembly with 30 bootstrap samples and an estimated fragment length of 200 ± 20 for single-end samples. For differential gene expression (DGE) analysis we aggregated reads of protein coding transcripts and used R (v. 4.0.3) with the package "edgeR" (v 3.32.1) for analysis. A filter was used to remove genes with low expression prior to DGE analysis. EdgeR was then used to calculate the normalization factors (TMM method) and estimate the dispersion (by weighted likelihood empirical Bayes). For two group comparisons the genewise exact test was used, for more complex designs we used a generalized linear model (GLM) with empirical Bayes quasi-likelihood F-tests. Exact specifications for each tested model can be found under https://github.com/ETHZ-INS/LC_Opto_Transcriptomics. For multiple testing correction the Benjamini-Hochberg false discovery rate (FDR) method was used, and for interaction terms (e.g. stress:sex or stress:injection), FDR was calculated only on the genes that have a significant stress effect. For analyses of data-sets originating from multiple experiments we further employed SVA correction to correct for processing specific effects (Leek et al. 2012). Surrogate variables independent of experimental groups were identified using the SVA package (v3.38.0) on data after DESeq2 (v1.30.1) variance-stabilization (Love, Huber, and Anders 2014), and were then included as additive terms in the GLMs. Heatmaps were produced with the sechm (v1.5.1) package. To avoid rare extreme values from driving the scale, the color scale is linear for values within a 98% interval, and ordinal for values outside it. Unless otherwise specified, the rows were sorted using the features' angle on a two-dimensional projection of the plotted values, as default in sechm.
For the combined analysis of consistent effects across yohimbine injection, chemogenetic and optogenetic stimulation we first combined all three datasets and modeled batch effects using SVA correction. We then designed a combined response variable that was set to control (homecage in the injection experiment, hM3Dq- in chemogenetic and ChR2- in optogenetic) or response (yohimbine in the injection experiment, hM3Dq+ in chemogenetic and ChR2+ in optogenetic). We then fit an additive generalized linear model with the newly defined response variable and the surrogate variables from the SVA correction and tested it for the response variable coefficient.
For the cumulative rank analysis, statistical results were used from multiple analyses (Stress group vs propranolol group in vHC of the first injection experiment; Stress group vs propranolol group in dHC of the first injection experiment; Stress:Propranolol interaction in second injection experiment; effect of chemogenetic LC activation in vHC; effect of chemogenetic LC activation in dHC; effect of optogenetic LC activation after 45 minutes). Then, in each analysis the gene with the lowest p-value was set to rank 1, the one with the highest to rank N. These ranks were then summed up across all analyses to generate the cumulative rank.

Reverse transcription quantitative real-time polymerase chain reaction (RT-qPCR)
Reactions were conducted using SYBR green (Roche) on a CFX384 Touch Real-Time PCR Detection System (Bio-Rad) and normalized against Tubulin delta 1 (Tubd1). Cycling conditions were 5 min at 95 °C, then 50 cycles with denaturation (10 s at 95 °C), annealing (10 s at 60 °C), and elongation (10 s at 72 °C). Primers were designed using PrimerBlast (Kozyreva et al. 2021) and tested for quality and specificity by melt-curve analysis, gel electrophoresis and appropriate negative controls. Forward (FP) and reverse (RP) primer sequences were as follows:

Tubd1: FP: TCTCTTGCTAACTTGGTGGTCCTC / RP: GCTGGGTCTTTAAATCCCTCTACG
Apold1: FP: ACCTCAGGCTCTCCTTCCATCATC / RP: ACCCGAGACAAAGCACCAATGC
Dio2: FP: GCCTACAAACAGGTTAAACTGGGTG / RP: CCATCAGCGGTCTTCTCC

Sik1: FP: ACAGCTCACTTCAGCCCTTAT / RP: CTCGCTGATAGCTGTGTCCA
Ppp1r3c: FP: TGAGCTGCACCAGAATGATCC / RP:GGTGGTGAATGAGCCAAGCA

Statistics

We used a block design for experiments. Animals and samples were split into multiple blocks, containing one replicate of each condition. Experimental and processing order within these blocks was randomized. Investigators were blinded during behavior and sample processing, but not during the analysis process. However, the same algorithmic analysis methods were used for all samples within each sequencing experiment. Analysis was performed in R or GraphPad Prism 9.2.0. For statistical analyses of behavior, pupillometry, immunohistochemistry and uHPLC data, we used independent samples t tests when comparing two independent groups. When comparing more than two groups we used one-way ANOVAs if there was a single independent variable, or two-way ANOVAs for two-factorial designs (e.g., injection x group). Significant main effects and interactions were analyzed using Tukey's post hoc tests. For linear model analysis we used the function lm() from the "stats" package in R and F-statistics for significance testing. No statistical method was used to predetermine sample size. No data were excluded from the analyses.

Data availability

The sequencing data data generated in this study has been deposited in the Gene Expression Omnibus database under accession code GSE218315 (reviewer token yhilwoocbhujjwp) for all injection experiments and GSE218313 for chemo and optogenetic experiments (reviewer token stoxiksgfhmpjiz).

Code availability

Code for all analyses (independent scripts) presented here is available on GitHub under https://github.com/ETHZ-INS/Privitera-et.-al.-2023.

Acknowledgments

The lab of JB was supported by the ETH Zurich, ETH Project Grant ETH-20 19-1, the Swiss National Science Foundation (grants 310030_172889/1 and 310030_204372), the Botnar Research Centre for Child Health, the Swiss 3R Competence Center, Roche, the Hochschulmedizin Zürich Flagship project STRESS, the Forschungskredit of the University of Zurich, the Novartis Foundation for Medical-Biological Research, the Swiss Foundation for Excellence and Talent in Biomedical Research, the Vontobel Foundation, the Betty and David Koetser Foundation for Brain Research. The lab of PPDD and DVD was supported by the University of Antwerp, Research Foundation Flanders (FWO), Joint Programming Initiative Neurodegenerative Diseases (JPND) and ZonMW (HEROES 73305172), Alzheimer Nederland and Neurosearch Antwerp. We thank the staff of the EPIC for the excellent animal care and their service to our animal facility and Prof. Isabelle Mansuy for providing support and space. We thank Han-Yu Lin and Justine Leonardi for help with sample processing and Julia Bode for maintaining the animal colony.

References

Allaman, I., L. Pellerin, and P. J. Magistretti. 2000. "Protein Targeting to Glycogen mRNA Expression Is Stimulated by Noradrenaline in Mouse Cortical Astrocytes." *Glia* 30 (4): 382–91.

Bangasser, Debra A., Samantha R. Eck, and Evelyn Ordoñes Sanchez. 2019. "Sex Differences in Stress Reactivity in Arousal and Attention Systems." *Neuropsychopharmacology: Official Publication of the American College of Neuropsychopharmacology* 44 (1): 129–39.

Benito, Eva, and Angel Barco. 2015. "The Neuronal Activity-Driven Transcriptome." *Molecular Neurobiology* 51 (3): 1071–88.

Bertorello, Alejandro Mario, and Jian-Kang Zhu. 2009. “SIK1/SOS2 Networks: Decoding Sodium Signals via Calcium-Responsive Protein Kinase Pathways.” *Pflugers Archiv: European Journal of Physiology* 458 (3): 613–19.

Bianco, Antonio C., Alexandra Dumitrescu, Balázs Gereben, Miriam O. Ribeiro, Tatiana L. Fonseca, Gustavo W. Fernandes, and Barbara M. L. C. Bocco. 2019. “Paradigms of Dynamic Control of Thyroid Hormone Signaling.” *Endocrine Reviews* 40 (4): 1000–1047.

Bohacek, Johannes, Francesca Manuella, Martin Roszkowski, and Isabelle M. Mansuy. 2015. “Hippocampal Gene Expression Induced by Cold Swim Stress Depends on Sex and Handling.” *Psychoneuroendocrinology* 52 (February): 1–12.

Bohmbach, Kirsten, Nicola Masala, Eva M. Schönhense, Katharina Hill, André N. Haubrich, Andreas Zimmer, Thoralf Opitz, Heinz Beck, and Christian Henneberger. 2022. “An Astrocytic Signaling Loop for Frequency-Dependent Control of Dendritic Integration and Spatial Learning.” *Nature Communications* 13 (1): 7932.

Bouret, Sebastien, and Susan J. Sara. 2002. “Locus Coeruleus Activation Modulates Firing Rate and Temporal Organization of Odour-Induced Single-Cell Responses in Rat Piriform Cortex.” *The European Journal of Neuroscience* 16 (12): 2371–82.

Bray, Nicolas L., Harold Pimentel, Páll Melsted, and Lior Pachter. 2016. “Near-Optimal Probabilistic RNA-Seq Quantification.” *Nature Biotechnology* 34 (5): 525–27.

Campos-Barros, A., H. Meinhold, M. Stula, F. Müller, R. Köhler, M. Eravci, O. Putzien, and A. Baumgartner. 1994. “The Influence of Desipramine on Thyroid Hormone Metabolism in Rat Brain.” *The Journal of Pharmacology and Experimental Therapeutics* 268 (3): 1143–52.

Cembrowski, Mark S., Julia L. Bachman, Lihua Wang, Ken Sugino, Brenda C. Shields, and Nelson Spruston. 2016. “Spatial Gene-Expression Gradients Underlie Prominent Heterogeneity of CA1 Pyramidal Neurons.” *Neuron* 89 (2): 351–68.

Coggan, Jay S., Daniel Keller, Corrado Calì, Heikki Lehväslaiho, Henry Markram, Felix Schürmann, and Pierre J. Magistretti. 2018. “Norepinephrine Stimulates Glycogenolysis in Astrocytes to Fuel Neurons with Lactate.” *PLoS Computational Biology* 14 (8): e1006392.

Dienel, Gerald A. 2017. “The Metabolic Trinity, Glucose-Glycogen-Lactate, Links Astrocytes and Neurons in Brain Energetics, Signaling, Memory, and Gene Expression.” *Neuroscience Letters* 637 (January): 18–25.

Endo, Fumito, Atsushi Kasai, Joselyn S. Soto, Xinzhu Yu, Zhe Qu, Hitoshi Hashimoto, Viviana Gradinaru, Riki Kawaguchi, and Baljit S. Khakh. 2022. “Molecular Basis of Astrocyte Diversity and Morphology across the CNS in Health and Disease.” *Science*. https://doi.org/10.1126/science.adc9020.

Feldman, J. D., L. Vician, M. Crispino, W. Hoe, M. Baudry, and H. R. Herschman. 2000. “The Salt-Inducible Kinase, SIK, Is Induced by Depolarization in Brain.” *Journal of Neurochemistry* 74 (6): 2227–38.

Feng, Jiesi, Changmei Zhang, Julieta E. Lischinsky, Miao Jing, Jingheng Zhou, Huan Wang, Yajun Zhang, et al. 2019. “A Genetically Encoded Fluorescent Sensor for Rapid and Specific In Vivo Detection of Norepinephrine.” *Neuron* 102 (4): 745–61.e8.

Fernandez-Albert, J., M. Lipinski, M. T. Lopez-Cascales, M. J. Rowley, A. M. Martin-Gonzalez, B. Del Blanco, V. G. Corces, and A. Barco. 2019. “Immediate and Deferred Epigenomic Signatures of in Vivo Neuronal Activation in Mouse Hippocampus.” *Nature Neuroscience* 22 (10). https://doi.org/10.1038/s41593-019-0476-2.

Fink, George. 2016. *Stress: Neuroendocrinology and Neurobiology: Handbook of Stress Series*. Academic Press.

Floriou-Servou, Amalia, Lukas M. von Ziegler, Rebecca Waag, Christa Schläppi, Pierre-Luc Germain, and Johannes Bohacek. 2021. “The Acute Stress Response in the Multiomic Era.” *Biological Psychiatry* 89 (12): 1116–26.

Floriou-Servou, Amalia, Lukas von Ziegler, Luzia Stalder, Oliver Sturman, Mattia Privitera, Anahita Rassi, Alessio Cremonesi, Beat Thöny, and Johannes Bohacek. 2018. “Distinct Proteomic, Transcriptomic, and Epigenetic Stress Responses in Dorsal and Ventral Hippocampus.” *Biological Psychiatry* 84 (7): 531–41.

Gao, Virginia, Akinobu Suzuki, Pierre J. Magistretti, Sylvain Lengacher, Gabriella Pollonini, Michael Q. Steinman, and Cristina M. Alberini. 2016. “Astrocytic β_2-Adrenergic Receptors Mediate Hippocampal Long-Term Memory Consolidation.” *Proceedings of the National Academy of Sciences of the United States of America* 113 (30): 8526–31.

Gerstner, Nathalie, Anthi C. Krontira, Cristiana Cruceanu, Simone Roeh, Benno Pütz, Susann Sauer, Monika Rex-Haffner, Mathias V. Schmidt, Elisabeth B. Binder, and Janine Knauer-Arloth. 2022. "DiffBrainNet: Differential Analyses Add New Insights into the Response to Glucocorticoids at the Level of Genes, Networks and Brain Regions." https://doi.org/10.1101/2022.04.21.489034.
Ghosh, Abhinaba, Faghihe Massaeli, Kyron D. Power, Tamunotonye Omoluabi, Sarah E. Torraville, Julia B. Pritchett, Tayebeh Sepahvand, et al. 2021. "Locus Coeruleus Activation Patterns Differentially Modulate Odor Discrimination Learning and Odor Valence in Rats." *Cerebral Cortex Communications* 2 (2): tgab026.
Gibbs, Marie E., Dana Hutchinson, and Leif Hertz. 2008. "Astrocytic Involvement in Learning and Memory Consolidation." *Neuroscience and Biobehavioral Reviews* 32 (5): 927–44.
Girgenti, Matthew J., Santosh Pothula, and Samuel S. Newton. 2021. "Stress and Its Impact on the Transcriptome." *Biological Psychiatry* 90 (2): 102–8.
Gray, J. D., T. G. Rubin, R. G. Hunter, and B. S. McEwen. 2013. "Hippocampal Gene Expression Changes Underlying Stress Sensitization and Recovery." *Molecular Psychiatry* 19 (11): 1171–78.
Grimm, Christina, Sian N. Duss, Mattia Privitera, Brandon R. Munn, Stefan Frässle, Maria Chernysheva, Tommaso Patriarchi, et al. 2022. "Locus Coeruleus Firing Patterns Selectively Modulate Brain Activity and Dynamics." *bioRxiv*. https://doi.org/10.1101/2022.08.29.505672.
Hansen, Niels. 2017. "The Longevity of Hippocampus-Dependent Memory Is Orchestrated by the Locus Coeruleus-Noradrenergic System." *Neural Plasticity* 2017 (June): 2727602.
Harley, Carolyn W., and Qi Yuan. 2021. "Locus Coeruleus Optogenetic Modulation: Lessons Learned from Temporal Patterns." *Brain Sciences* 11 (12). https://doi.org/10.3390/brainsci11121624.
Hermans, Erno J., Marloes J. A. G. Henckens, Marian Joëls, and Guillén Fernández. 2014. "Dynamic Adaptation of Large-Scale Brain Networks in Response to Acute Stressors." *Trends in Neurosciences* 37 (6): 304–14.
Hirschberg, Stefan, Yong Li, Andrew Randall, Eric J. Kremer, and Anthony E. Pickering. 2017. "Functional Dichotomy in Spinal- vs Prefrontal-Projecting Locus Coeruleus Modules Splits Descending Noradrenergic Analgesia from Ascending Aversion and Anxiety in Rats." *eLife* 6 (October). https://doi.org/10.7554/eLife.29808.
Huang, Bing S., Roselyn A. White, and Frans H. H. Leenen. 2012. "Possible Role of Brain Salt-Inducible Kinase 1 in Responses to Central Sodium in Dahl Rats." *American Journal of Physiology-Regulatory, Integrative and Comparative Physiology*, July. https://doi.org/10.1152/ajpregu.00381.2011.
Iqbal, Zafar, Zhuogui Lei, Aruna S. Ramkrishnan, Shu Liu, Mahadi Hasan, Mastura Akter, Yuk Yan Lam, and Ying Li. 2023. "Adrenergic Signalling to Astrocytes in Anterior Cingulate Cortex Contributes to Pain-Related Aversive Memory in Rats." *Communications Biology* 6 (1): 10.
Jaitovich, Ariel, and Alejandro M. Bertorello. 2010. "Intracellular Sodium Sensing: SIK1 Network, Hormone Action and High Blood Pressure." *Biochimica et Biophysica Acta* 1802 (12): 1140–49.
Joëls, Marian, and Tallie Z. Baram. 2009. "The Neuro-Symphony of Stress." *Nature Reviews. Neuroscience* 10 (6): 459–66.
Johnston, A. L., H. A. Baldwin, and S. E. File. 1988. "Measures of Anxiety and Stress in the Rat Following Chronic Treatment with Yohimbine." *Journal of Psychopharmacology* 2 (1): 33–38.
Kagiampaki, Zacharoula, Valentin Rohner, Cedric Kiss, Sebastiano Curreli, Alexander Dieter, Maria Wilhelm, Masaya Harada, et al. 2023. "Sensitive Multicolor Indicators for Monitoring Norepinephrine in Vivo." *Nature Methods* 20 (9): 1426–36.
Kozyreva, A. A., A. M. Zlotina, A. S. Golovkin, O. V. Kalinina, and A. A. Kostareva. 2021. "Primer Designing in Primer-BLAST." *Translational Medicine*. https://doi.org/10.18705/2311-4495-2021-8-3-37-52.
Leek, Jeffrey T., W. Evan Johnson, Hilary S. Parker, Andrew E. Jaffe, and John D. Storey. 2012. "The Sva Package for Removing Batch Effects and Other Unwanted Variation in High-Throughput Experiments." *Bioinformatics*. https://doi.org/10.1093/bioinformatics/bts034.
Leibowitz, S. F., C. Sladek, L. Spencer, and D. Tempel. 1988. "Neuropeptide Y, Epinephrine and Norepinephrine in the Paraventricular Nucleus: Stimulation of Feeding and the Release of Corticosterone, Vasopressin and Glucose." *Brain Research Bulletin* 21 (6): 905–12.
Likhtik, Ekaterina, and Joshua P. Johansen. 2019. "Neuromodulation in Circuits of Aversive Emotional Learning." *Nature Neuroscience* 22 (10): 1586–97.
Love, Michael I., Wolfgang Huber, and Simon Anders. 2014. "Moderated Estimation of Fold Change and Dispersion for RNA-Seq Data with DESeq2." *Genome Biology* 15 (12): 550.

Loy, Rebekah, David A. Koziell, James D. Lindsey, and Robert Y. Moore. 1980. “Noradrenergic Innervation of the Adult Rat Hippocampal Formation.” *The Journal of Comparative Neurology*. https://doi.org/10.1002/cne.901890406.
Martin, Marcel. 2011. “Cutadapt Removes Adapter Sequences from High-Throughput Sequencing Reads.” *EMBnet.journal* 17 (1): 10–12.
Mather, Mara, David Clewett, Michiko Sakaki, and Carolyn W. Harley. 2016. “GANEing Traction: The Broad Applicability of NE Hotspots to Diverse Cognitive and Arousal Phenomena.” *The Behavioral and Brain Sciences* 39 (January): e228.
McCall, Jordan G., Ream Al-Hasani, Edward R. Siuda, Daniel Y. Hong, Aaron J. Norris, Christopher P. Ford, and Michael R. Bruchas. 2015. “CRH Engagement of the Locus Coeruleus Noradrenergic System Mediates Stress-Induced Anxiety.” *Neuron* 87 (3): 605–20.
McCall, Jordan G., Edward R. Siuda, Dionnet L. Bhatti, Lamley A. Lawson, Zoe A. McElligott, Garret D. Stuber, and Michael R. Bruchas. 2017. “Locus Coeruleus to Basolateral Amygdala Noradrenergic Projections Promote Anxiety-like Behavior.” *eLife* 6 (July). https://doi.org/10.7554/eLife.18247.
McGaugh, James L., and Benno Roozendaal. 2002. “Role of Adrenal Stress Hormones in Forming Lasting Memories in the Brain.” *Current Opinion in Neurobiology* 12 (2): 205–10.
Meijer, Onno C., Jacobus C. Buurstede, Eva M. G. Viho, Jorge Miguel Amaya, Anne-Sophie C. A. M. Koning, Merel van der Meulen, Lisa T. C. M. van Weert, Susana N. Paul, Jan Kroon, and Lisa L. Koorneef. 2022. “Transcriptional Glucocorticoid Effects in the Brain: Finding the Relevant Target Genes.” *Journal of Neuroendocrinology*, November, e13213.
Mifsud, Karen R., Clare L. M. Kennedy, Silvia Salatino, Eshita Sharma, Emily M. Price, Samantha N. Haque, Andriana Gialeli, et al. 2021. “Distinct Regulation of Hippocampal Neuroplasticity and Ciliary Genes by Corticosteroid Receptors.” *Nature Communications* 12 (1): 1–23.
Murphy-Royal, Ciaran, April D. Johnston, Andrew K. J. Boyce, Blanca Diaz-Castro, Adam Institoris, Govind Peringod, Oliver Zhang, et al. 2020. “Stress Gates an Astrocytic Energy Reservoir to Impair Synaptic Plasticity.” *Nature Communications* 11 (1): 2014.
O’Donnell, John, Fengfei Ding, and Maiken Nedergaard. 2015. “Distinct Functional States of Astrocytes during Sleep and Wakefulness: Is Norepinephrine the Master Regulator?” *Current Sleep Medicine Reports* 1 (1): 1–8.
Oleskevich, S., L. Descarries, and J. C. Lacaille. 1989. “Quantified Distribution of the Noradrenaline Innervation in the Hippocampus of Adult Rat.” *The Journal of Neuroscience: The Official Journal of the Society for Neuroscience* 9 (11): 3803–15.
Oyarzabal, Esteban A., Li-Ming Hsu, Manasmita Das, Tzu-Hao Harry Chao, Jingheng Zhou, Sheng Song, Weiting Zhang, et al. 2022. “Chemogenetic Stimulation of Tonic Locus Coeruleus Activity Strengthens the Default Mode Network.” *Science Advances* 8 (17): eabm9898.
Paillasse, Michael R., and Philippe de Medina. 2015. “The NR4A Nuclear Receptors as Potential Targets for Anti-Aging Interventions.” *Medical Hypotheses* 84 (2): 135–40.
Pan, Jie, Nana Ma, Jie Zhong, Bo Yu, Jun Wan, and Wei Zhang. 2021. “Age-Associated Changes in Microglia and Astrocytes Ameliorate Blood-Brain Barrier Dysfunction.” *Molecular Therapy. Nucleic Acids* 26 (December): 970–86.
Petit, J-M, E. Eren-Koçak, H. Karatas, P. Magistretti, and T. Dalkara. 2021. “Brain Glycogen Metabolism: A Possible Link between Sleep Disturbances, Headache and Depression.” *Sleep Medicine Reviews* 59 (October): 101449.
Poe, Gina R., Stephen Foote, Oxana Eschenko, Joshua P. Johansen, Sebastien Bouret, Gary Aston-Jones, Carolyn W. Harley, et al. 2020. “Locus Coeruleus: A New Look at the Blue Spot.” *Nature Reviews Neuroscience*. https://doi.org/10.1038/s41583-020-0360-9.
Popichak, Katriana A., Sean L. Hammond, Julie A. Moreno, Maryam F. Afzali, Donald S. Backos, Richard D. Slayden, Stephen Safe, and Ronald B. Tjalkens. 2018. “Compensatory Expression of Nur77 and Nurr1 Regulates NF-κB-Dependent Inflammatory Signaling in Astrocytes.” *Molecular Pharmacology* 94 (4): 1174–86.
Privitera, Mattia, Kim David Ferrari, Lukas M. von Ziegler, Oliver Sturman, Sian N. Duss, Amalia Floriou-Servou, Pierre-Luc Germain, et al. 2020. “A Complete Pupillometry Toolbox for Real-Time Monitoring of Locus Coeruleus Activity in Rodents.” *Nature Protocols* 15 (8): 2301–20.
Rivas, M., and J. R. Naranjo. 2007. “Thyroid Hormones, Learning and Memory.” *Genes, Brain, and Behavior* 6 Suppl 1 (June): 40–44.
Robertson, Sabrina D., Nicholas W. Plummer, Jacqueline de Marchena, and Patricia Jensen. 2013.

"Developmental Origins of Central Norepinephrine Neuron Diversity." *Nature Neuroscience* 16 (8): 1016–23.
Roszkowski, Martin, Francesca Manuella, Lukas von Ziegler, Gonzalo Durán-Pacheco, Jean-Luc Moreau, Isabelle M. Mansuy, and Johannes Bohacek. 2016. "Rapid Stress-Induced Transcriptomic Changes in the Brain Depend on Beta-Adrenergic Signaling." *Neuropharmacology* 107 (August): 329–38.
Rubin, Todd G., Jason D. Gray, and Bruce S. McEwen. 2014. "Experience and the Ever-Changing Brain: What the Transcriptome Can Reveal." *BioEssays: News and Reviews in Molecular, Cellular and Developmental Biology* 36 (11): 1072–81.
Sara, Susan J. 2015. "Locus Coeruleus in Time with the Making of Memories." *Current Opinion in Neurobiology* 35 (December): 87–94.
Schwabe, Lars, Erno J. Hermans, Marian Joëls, and Benno Roozendaal. 2022. "Mechanisms of Memory under Stress." *Neuron*. https://doi.org/10.1016/j.neuron.2022.02.020.
Smith, M. A., S. Banerjee, P. W. Gold, and J. Glowa. 1992. "Induction of c-Fos mRNA in Rat Brain by Conditioned and Unconditioned Stressors." *Brain Research* 578 (1-2): 135–41.
Stankiewicz, Adrian M., Joanna Goscik, Alicja Majewska, Artur H. Swiergiel, and Grzegorz R. Juszczak. 2015. "The Effect of Acute and Chronic Social Stress on the Hippocampal Transcriptome in Mice." *PloS One* 10 (11): e0142195.
Strange, Bryan A., Menno P. Witter, Ed S. Lein, and Edvard I. Moser. 2014. "Functional Organization of the Hippocampal Longitudinal Axis." *Nature Reviews. Neuroscience* 15 (10): 655–69.
Sturman, Oliver, Pierre-Luc Germain, and Johannes Bohacek. 2018. "Exploratory Rearing: A Context- and Stress-Sensitive Behavior Recorded in the Open-Field Test." *Stress* 21 (5): 443–52.
Sui, L., F. Wang, F. Liu, J. Wang, and B. M. Li. 2006. "Dorsal Hippocampal Administration of Triiodothyronine Enhances Long-Term Memory for Trace Cued and Delay Contextual Fear Conditioning in Rats." *Journal of Neuroendocrinology* 18 (11): 811–19.
Tyssowski, K. M., N. R. DeStefino, J. H. Cho, C. J. Dunn, C. E. Carty, R. D. Jones, S. M. Chang, et al. 2018. "Different Neuronal Activity Patterns Induce Different Gene Expression Programs." *Neuron* 98 (3). https://doi.org/10.1016/j.neuron.2018.04.001.
Uematsu, Akira, Bao Zhen Tan, and Joshua P. Johansen. 2015. "Projection Specificity in Heterogeneous Locus Coeruleus Cell Populations: Implications for Learning and Memory." *Learning & Memory* 22 (9): 444–51.
Villain, Hélène, Aïcha Benkahoul, Philippe Birmes, Barbara Ferry, and Pascal Roullet. 2018. "Influence of Early Stress on Memory Reconsolidation: Implications for Post-Traumatic Stress Disorder Treatment." *PloS One* 13 (1): e0191563.
Wang, C., D. Song, J. Fu, and X. Wen. 2020. "SIK1 Regulates CRTC2-Mediated Gluconeogenesis Signaling Pathway in Human and Mouse Liver Cells." *Frontiers in Endocrinology* 11 (September). https://doi.org/10.3389/fendo.2020.00580.
Xu, Liming, Mo Dan, Anliang Shao, Xiang Cheng, Cuiping Zhang, Robert A. Yokel, Taro Takemura, Nobutaka Hanagata, Masami Niwa, and Daisuke Watanabe. 2015. "Silver Nanoparticles Induce Tight Junction Disruption and Astrocyte Neurotoxicity in a Rat Blood-Brain Barrier Primary Triple Coculture Model." *International Journal of Nanomedicine* 10 (September): 6105–18.
Zenger, Manuel, Sophie Burlet-Godinot, Jean-Marie Petit, and Pierre J. Magistretti. 2017. "Chapter 9 - Noradrenergic System and Memory: The Role of Astrocytes." In *Noradrenergic Signaling and Astroglia*, edited by Nina Vardjan and Robert Zorec, 183–200. Academic Press.
Zerbi, Valerio, Amalia Floriou-Servou, Marija Markicevic, Yannick Vermeiren, Oliver Sturman, Mattia Privitera, Lukas von Ziegler, et al. 2019. "Rapid Reconfiguration of the Functional Connectome after Chemogenetic Locus Coeruleus Activation." *Neuron* 103 (4): 702–18.e5.
Zhu, Anqi, Joseph G. Ibrahim, and Michael I. Love. 2018. "Heavy-Tailed Prior Distributions for Sequence Count Data: Removing the Noise and Preserving Large Differences." *Bioinformatics* 35 (12): 2084–92.
Zhu, Hu, Dipendra K. Aryal, Reid H. J. Olsen, Daniel J. Urban, Amanda Swearingen, Stacy Forbes, Bryan L. Roth, and Ute Hochgeschwender. 2016. "Cre-Dependent DREADD (Designer Receptors Exclusively Activated by Designer Drugs) Mice." *Genesis* 54 (8): 439–46.
Ziegler, Lukas M. von, Amalia Floriou-Servou, Rebecca Waag, Rebecca R. Das Gupta, Oliver Sturman, Katharina Gapp, Christina A. Maat, et al. 2022. "Multiomic Profiling of the Acute Stress Response in the Mouse Hippocampus." *Nature Communications* 13 (1): 1824.